COMPOSTION OF FLUID INCLUSIONS FROM THE CAVE-IN-ROCK BEDDED-REPLACEMENT FLUORITE DEPOSITS IN THE ILLINOIS-KENTUCKY DISTRICT

A Thesis

presented to

the Faculty of the Graduate School

at the University of Missouri-Columbia

In Partial Fulfillment

of the Requirements for the Degree

Master of Science

---

by

MICHAEL A. PELCH

Dr. Martin Appold, Thesis Supervisor

July 2011

The undersigned, appointed by the dean of the Graduate School,

have examined the thesis entitled

COMPOSTION OF FLUID INCLUSIONS FROM THE CAVE-IN-ROCK BEDDED-REPLACEMENT FLUORITE DEPOSITS IN THE ILLINOIS-KENTUCKY DISTRICT

Presented by Michael A. Pelch,

A candidate for the degree of

Master of Science

And hereby certify that, in their opinion, it is worthy of acceptance.

_____

Dr. Kevin L. Shelton

_____

Dr. Martin S. Appold

_____

Dr. Michael D. Glascock

Acknowledgements

First I would like to acknowledge and thank my advisor, Dr. Martin Appold, for his mentorship, guidance, revision, and financial support of this project. I would like to thank my committee members, Dr. Kevin Shelton and Dr. Michael Glascock, for their additional revisions and input on my project. I would like to acknowledge the Department of Geological Sciences at the University of Missouri for supporting my Masters work financially from the Fred Strothmann and Lillie M. Carter scholarships. I would also like to thank Dr. Luca Fedele from Virginia Tech for his excellent technical knowledge and insight into the successful laser ablation of fluorite-hosted fluid inclusions, and to Zachary Wenz for assisting me on many occasions on improving sample preparation and providing additional insight and knowledge about Mississippi Valley-type ore deposits. I would like to acknowledge the Society of Economic Geologists for supplying research funding that supported part of the sample analyses in this research. I also want to thank Dr. Paul Spry of Iowa State University, Ross Lillie of North Star Minerals, and Ray Guillemette of the Illinois State Geological Survey for generously supplying mineral samples from the Illinois-Kentucky district, and the USGS Columbia Environmental Research Center and Dr. Al Hofstra of USGS Denver for assisting in performing ion chromatography on several mineral samples. Finally, I would like to thank my wife for all of the moral support and graduate school advice that was key to my success over the last several years, and my parents who always fostered my interest in science.

Table of Contents

List of Figures

List of Tables

Abstract

The stable mid-continent platform of North America hosts some of the greatest known concentrations of Mississippi Valley-type (MVT) mineralization in the world. Most of the mineralization occurs between two major physiographic regions, the Ozark Plateau and the Interior Low Plateau. The Illinois-Kentucky district, which is the focus of the present study, is one of three principal MVT districts in the Interior Low Plateau and is distinct from other North American mid-continent MVT deposits in that its ore mineral assemblage is dominated by fluorite instead of sulfide minerals or barite. However, like these other MVT deposits, the Illinois-Kentucky deposits were probably precipitated from northward flowing sedimentary brines set in motion by topographic gradients created by the Alleghanian-Ouachita orogeny during the Late Paleozoic. The primary objective of the current study was to quantify the chemical composition of the mineralizing fluids through in situ fluid inclusion analysis using microthermometry, laser ablation-inductively coupled plasma-mass spectrometry (LA-ICP-MS), and laser Raman spectroscopy in order to try to gain insights into the ore formation process. The samples studied were all from bedded replacement deposits in the Cave-in-Rock subdistrict.

Results from this study show that the fluids that formed the Illinois-Kentucky district are chemically distinct from the fluids that formed MVT deposits in the adjacent Ozark Plateau. These differences can be attributed to interaction of the mineralizing sedimentary brines with ultramafic, rift-related igneous rocks present in the Illinois-Kentucky district but not in any of the Ozark Plateau MVT districts. Fluid inclusion homogenization temperature and salinity relationships suggest that MVT mineralization in the Illinois-Kentucky district was produced from a mixture of at least three brines, two of which had relatively high salinities and temperatures and the third of which was considerably more dilute and cooler. Mixing among at least three fluids is supported by the elemental concentration data, which tend not to correlate with one another or with the microthermometry data, but rather plot as scattered two-dimensional arrays. The compositions of the end member fluids could not be pinpointed from the available

data, however it appears that at least one of the fluids had elevated concentrations of the ore metals, Pb, Zn, Cu, and Fe as high as on the order of 1000's of ppm. Raman microprobe analyses were used to quantify methane concentrations in fluid inclusions, from which fluid inclusion trapping pressures and depths of mineralization could be calculated, which varied widely, mainly from about 100 to 1500 m with a mean of 680 m. The higher depth values in this range are more consistent with published erosional unloading histories for the Illinois-Kentucky region, suggesting that the fluid inclusions that yielded lower depth of mineralization values had stretched since entrapment or were not truly saturated with respect to methane as was assumed in the calculation.

Introduction

The stable mid-continent platform of North America hosts some of the greatest known concentrations of Mississippi Valley-type (MVT) mineralization in the world. Most of the mineralization is distributed among two physiographic provinces, the Ozark Plateau in the west and the Interior Low Plateau in the east (Figure 1). The Ozark Plateau contains four distinct districts of sulfide and/or barite mineralization, including the giant Southeast Missouri and Tri-State districts. The Interior Low Plateau contains three distinct districts of fluorite and sulfide mineralization, including the Illinois-Kentucky district, which is the focus of this study.

Most of the MVT mineralization in both the Ozark and Interior Low Plateau is probably genetically related to a northward flowing, topographically driven, groundwater system that was initiated by the Alleghanian-Ouachita orogeny during the Late Paleozoic. The chemical composition of this groundwater in the Ozark Plateau has been profiled in studies by Viets and Leach (1990), Kendrick et al. (2002), Appold et al. (2004), Stoffel et al. (2008), Shelton et al. (2009), Appold and Wenz (2011), and Wenz (2011). These studies have shown that the groundwater is similar in composition to modern sedimentary brines with salinities ranging from 16-24 equivalent weight percent (eq. wt%) NaCl, total dissolved solids (TDS) contents of 217,000 parts per million (ppm), and major cation concentrations of Na = 65,379 ppm, Ca = 17,730 ppm, Mg = 1968 ppm, K = 2863 ppm, and Sr = 686 ppm (Wenz, 2011). The groundwater was consistently dolomitizing and had elevated concentrations of K relative to typical sedimentary brines. The groundwater had methane concentrations approaching several hundred ppm, implying generally reducing environmental conditions and burial depths for mineralization between 0.08 and 1.3 km. All four of the Ozark MVT districts have a population of sphalerite-hosted fluid inclusions with high Pb concentrations on the order of 100's to 1000's of ppm. These high concentrations probably indicate that some of the groundwater entering the MVT districts was Pb and possibly overall metal-rich, and mixed with metal-poor, possibly sulfur-rich

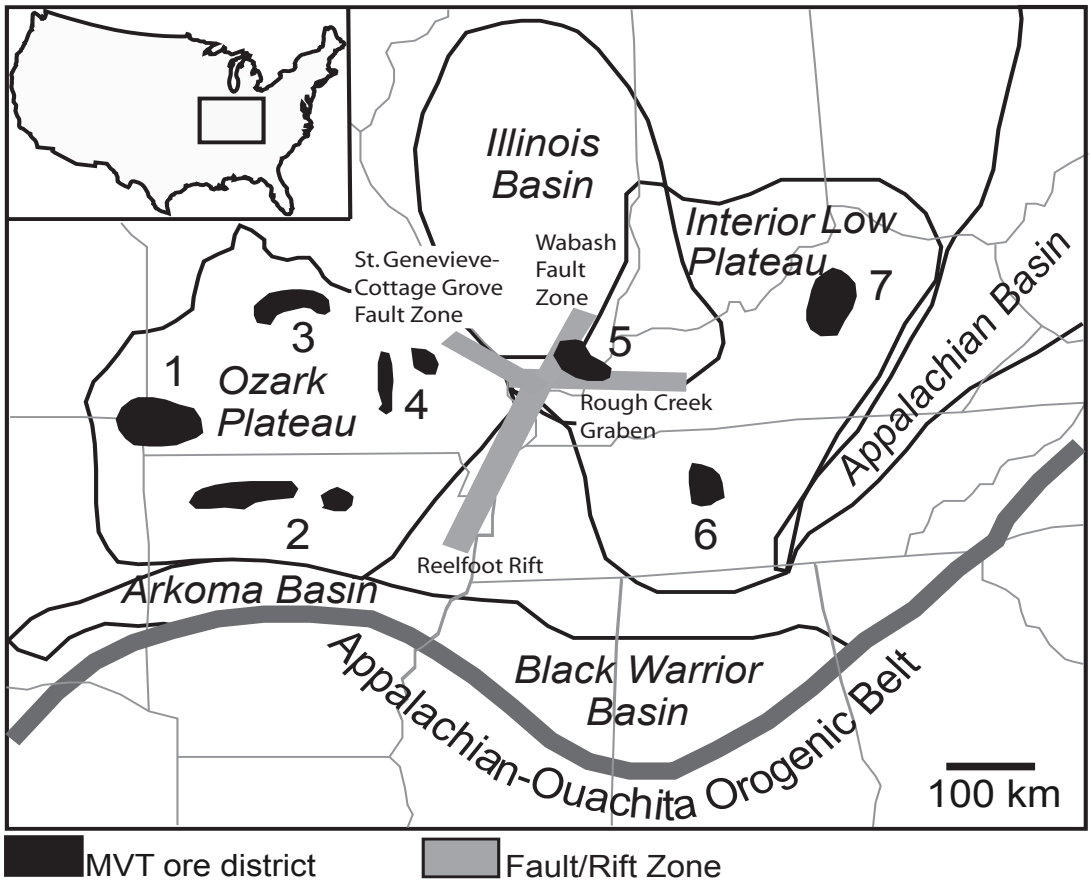

Figure 1: Map showing the locations of MVT districts in the Interior Low Plateau, Ozark Plateau, and major geologic features. Tri-State district (1), Northern Arkansas district (2), Central Missouri district (3), Southeast Missouri district (4), Illinois-Kentucky district (5), Central Tennessee district (6), Central Kentucky district (7). This figure is modified from Appold and Wenz (2011).

fluid. Unfortunately, the concentrations of other ore metals, Zn and Cu, could not be determined in the sphalerite hosted fluids inclusions due to high host mineral matrix interference and neither Pb, Zn, nor Cu was ever detected in fluid inclusions hosted by dolomite, quartz, or calcite gangue. Consequently, Zn and Cu concentrations from the MVT mineralizing fluid remain unknown. However, Ba was found to exist in concentrations on the order of 1's to 100's of ppm.

Less is known about the composition of MVT mineralizing fluids in the Interior Low Plateau. For the Illinois-Kentucky district, most of what has been learned has come from microthermomtery and bulk crush leachate analysis of fluid inclusions. Microthermometry studies have been carried out by Grogan and Shrode (1952), Hall and Friedman (1963), Horn and Amstutz (1978), Cunningham and Heyl (1980), Richardson and Pinckney (1984), Spry and Fuhrmann (1990), Spry et al. (1990), and Fuhrmann (1994). Most of the mineralization has fluid inclusion homogenization temperatures in the range of about 110 to 150 °C. Homogenization temperatures tend towards the higher end of this range in the middle parts of the paragenesis and toward the lower end of this range in the latest parts of the paragenesis. Fluid inclusion salinities in main-stage mineralization range mostly between 17 and 24 eq. wt% NaCl, though, salinities of 0 to 9 eq. wt% NaCl have been reported from some of the latest stage mineralization. First ice melting temperatures commonly range between -55.0 and -50.0 °C indicating the presence of other salts besides NaCl in the fluid inclusions, particularly $CaCl_2$.

Several previous studies have attempted to determine the composition of mineralizing fluids in the Illinois-Kentucky district from bulk crush leachate analysis. Czamanske et al. (1963) used neutron activation to analyze leachates from fluid inclusions hosted in fluorite and obtained Zn concentrations of 10,900 ppm and Cu concentrations of 9100 ppm. Pinckney and Haffty (1970) used atomic absorption spectrometry to analyze leachates from fluid inclusions hosted by fluorite, quartz, and barite. They found Zn concentrations to be highest in paragenetically early yellow and purple fluorite at 90-1040 ppm, lower in intermediate quartz at 60-340 ppm, and lowest in paragenetically late barite at 20-280 ppm. When detected, Cu concentrations were on

the order of 100's of ppm, with a maximum of 350 ppm in quartz hosted fluid inclusions. Hall and Friedman (1963) used flame photometry and colorimetry to measure the major element composition of fluid inclusions hosted by fluorite, quartz, sphalerite, galena, barite, and witherite. They determined that the mineralization was deposited by concentrated Na-Ca-Cl-type water, similar in composition to an oil field brine. Paragenetically earlier mineralization was found to contain higher concentrations (between 140,000 and 165,000 ppm) of soluble salts than later mineralization (between 6,000 and 100,000 ppm).

The primary objective of the present study was to characterize more rigorously the compositions of fluids involved in the formation of MVT deposits in the Illinois-Kentucky district in order to provide stronger constraints on the deposits' origin. Since the pioneering studies of Czamanske et al. (1963), Hall and Friedman (1963), and Pinckney and Haffty (1970), great progress has been made in the development of methods for in situ analysis of individual fluid inclusions using laser ablation-inductively coupled plasma-mass spectrometry (LA-ICP-MS) and Raman spectroscopy. In particular, LA-ICP-MS offers the opportunity to determine the concentrations of ore metals like Pb, Zn, Cu, and Ba in fluid inclusions with much greater certainty that analyses based on bulk analytical methods because sulfide and barite mineral inclusions that could contaminate the fluid inclusion signal can be more easily recognized and avoided.

The present study focuses on using LA-ICP-MS to profile the composition of fluid inclusions from across the paragenesis of bedded replacement fluorite deposits from the Cave-in-Rock sub-district of the Illinois-Kentucky district. Raman microprobe analysis was used to determine methane concentrations in fluid inclusions, from which mineral trapping pressures could be computed. Unfortunately, neither LA-ICP-MS nor Raman spectroscopy can be used to determine the concentration of F in solution, one of the two main constituents of the main ore mineral, fluorite.

The results of this study allow several specific research questions to be addressed

including: (1) How does the composition of the Illinois-Kentucky ore fluids compare to that of typical sedimentary brines and MVT ore fluids, particularly the adjacent Ozark Plateau? (2) At what depth did the MVT mineralization in the Illinois-Kentucky district form? (3) Were there any temporal variations in the composition of the Illinois-Kentucky ore fluids? (4) What was the mechanism of ore precipitation?

Geologic Background

The geology of the Illinois-Kentucky district has been described by Bastin (1931), Weller et al. (1952), Brown et al. (1954), Heyl and Brock (1965), Trace (1974), Heyl (1983), Baxter and Bradbury (1989), and Goldstein (1997), from which the following summary has been derived. The district is located near the southern margin and depocenter of the Illinois basin, near the intersection of the Reelfoot Rift and Rough Creek Graben (Figure 1). MVT mineralization occurs over a wide interval of Mississippian-age sedimentary rocks, consisting primarily of limestone with lesser interbedded sandstone and shale that represent a near-shore marine and deltaic environment. Underlying the Mississippian sedimentary rocks are approximately 4 km of Paleozoic-shelf deposits that are generally interpreted to have been deposited in deeper water and have a higher proportion of carbonate to clastic rock, with the limestones mostly having been converted to dolomite. The Mississippian rocks of the district are overlain by approximately 0.5 km of Pennsylvanian to Quaternary-aged sedimentary rocks comprised mostly of coarse clasts.

The sedimentary rocks of the district have been deformed into a northwest-trending domal anticline named the Tolu Arch and by a series of northeast-trending normal faults. These structures are interpreted to be the result of uplift caused by an igneous intrusion, perhaps as a result of reactivation of the Reelfoot Rift and Rough Creek Graben some time during the Late Paleozoic collision and Mesozoic rifting of North America and Gondwanaland. Support for the existence of this intrusion comes from numerous ultramafic dikes and sills found within the district, and from Hicks Dome, a cryptovolcanic explosive igneous structure inferred from a radially oriented pattern of variably mineralized faults and fractures that forms the structural apex

of the district. Most of the igneous dikes and sills have been partially altered to serpentine, carbonate, and silica but are thought originally to have been mica peridotites and lamprophyres (Bradbury, 1962).

Deposit Types

Four major types of mineral deposits are recognized in the Illinois-Kentucky district: vein, bedded replacement, breccia, and residual deposits. Vein deposits account for most of the mineralization in the district. They occur predominantly as fillings in steeply dipping northeast trending normal faults and to a lesser extent in fractures and fissures. Veins can vary in thickness from less than a millimeter to as wide as 15m, though most range from 30 cm to 5 m. The strike lengths of vein deposits are typically between 8 and 120 m, with a maximum of over 1700 m, and the vertical extents of vein deposits are typically between 30 and 60 m, with a maximum of nearly 250 m (Grogan and Bradbury, 1968).

Bedded replacement deposits occur as replacements of their host rock parallel to bedding. Bedded replacement deposits are restricted geographically mostly to the Cave-in-Rock subdistrict in Illinois, with a second, smaller and less studied occurrence near Carrsville, Kentucky (Grogan and Bradbury, 1968). Compared to vein deposits, bedded replacement deposits are restricted to a much narrower stratigraphic interval of Mississippian host rocks, which are mainly oolitic or fossiliferous limestones overlain by shaley sandstones, representing a transition from a shallow near-shore environment to a deep-water marine environment. The deposits are typically associated with steeply dipping faults and fractures that may have acted as feeders for mineralizing fluids. As fluids rising along these feeder faults and fractures reached the shaley sandstone aquitards they were driven laterally into the more permeable oolitic and fossiliferous limestones that they replaced with MVT mineralization. Individual deposits are typically 15 to 50 m wide 1.5 to 6 m thick and 60m to 3 km long. Fluorite in bedded replacement deposits commonly displays a characteristic pattern of alternating coarse, light-colored bands and fine-grained, dark colored bands referred to as “coontail” ore. A further characteristic of bedded

replacement deposits is solution thinning of their host rock which has caused slumping of the overlying rocks.

Numerous intrusive breccia bodies occur in the vicinity of Hicks Dome. These breccia bodies can be as long as 250 m and over 150 m in height. A few of the breccia bodies have been mineralized with fluorite, sulfides, and barite. Fluorite from the breccia deposits is significantly enriched in rare earth elements, which also occur in bertrendite, brockite, florencite, monazite, rutile, and xenotime.

Residual deposits are the weathered remains of older ore deposits particularly vein deposits. The deposits can be as much as 18 m wide and consist of clasts of fluorite and host rock in a clay-rich matrix.

Mineralogy and Paragenesis

The Illinois-Kentucky district contains a mineral assemblage of fluorite, sphalerite, galena, barite, quartz, and calcite that is typical of MVT deposits but unusual with respect to the predominance of fluorite. In the Cave-in-Rock subdistrict four distinct episodes of hydrothermal activity are recognized (Figure 2; Richardson and Pinckney, 1984). Episode I is characterized by limestone dissolution and brecciation during which no hydrothermal mineral precipitation occurred. Episode II marks the beginning of hydrothermal mineral precipitation, during which an early yellow fluorite (Y1), followed by a band of purple fluorite (P1) and then another band of yellow fluorite (Y2) were deposited. The first calcite, typically a white, rhombohedral form, and minor dolomite, siderite, and chalcopyrite were also precipitated during late episode II. Episode III represents the main stage of MVT mineralization. Six distinct bands of purple fluorite (P2-P7) were precipitated during this time. Sphalerite, galena, quartz, and additional chalcopyrite were precipitated during the early stages of episode III, overlapping mainly P2 and P3 fluorite precipitation. Hydrothermal activity ended with episode IV, during which barite, witherite, and yellow-brown scalenohedral calcite were precipitated.

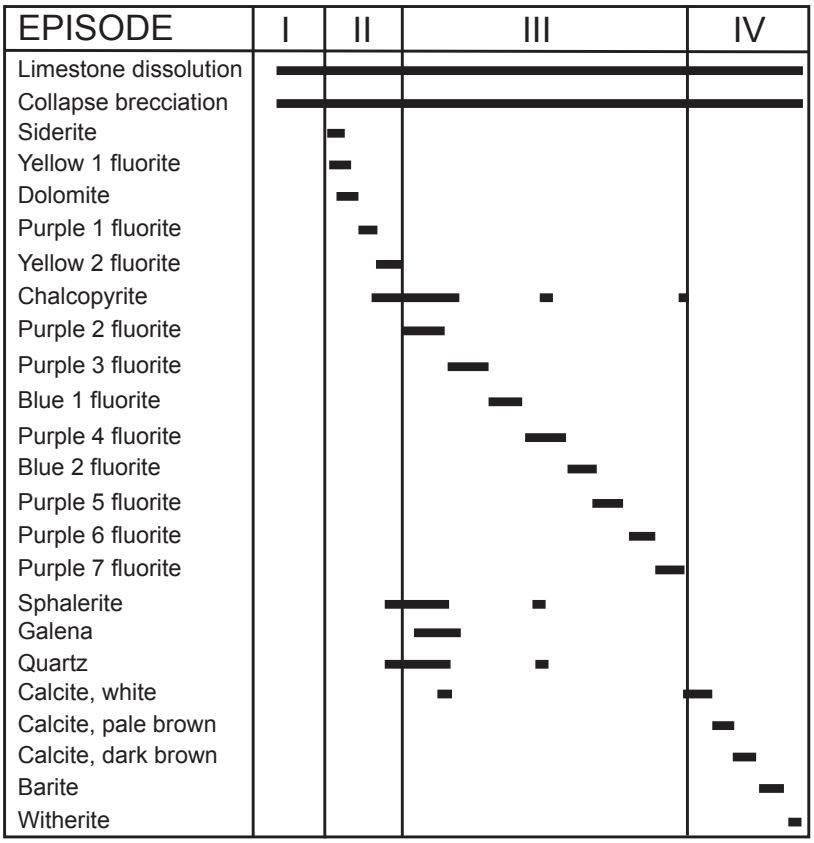

Figure 2: Mineral paragenesis for bedded replacement fluorite deposits defined by Richardson and Pinckney (1984).

Age of Mineralization

The age of mineralization in the Illinois-Kentucky district has not yet been clearly established. Field relations constrain the age of mineralization to be between Pennsylvanian and Upper Cretaceous, as mineralized faults have displaced strata of this age range (Grogan and Brabury, 1968), and clasts of fluorite occur in Cretaceous gravels of the Mississippi embayment (A.V. Heyl oral communication, 1985, cited in Richardson et al., 1988). Mineralization has long been thought be related to ultramafic igneous activity in the district. Attempts by Zartman et al. (1967) and Snee and Hayes (1992) to date this activity using the K-Ar, Rb-Sr, and Ar-Ar methods have yielded Permian ages in the range of 258±13 Ma to 281±14 Ma.

Several attempts have been made to date the age of mineralization directly. Ruiz et al. (1988) measured the $^{87}Sr/^{86}Sr$ ratio in fluorites from the Cave-in-Rock subdistrict. Comparing this ratio to the theoretical evolution of $^{87}Sr/^{86}Sr$ in biotite from Permian igneous rocks analyzed by Zartman et al. (1967), Ruiz et al. (1988) estimated an early Jurassic age of about 200 Ma for the fluorite assuming that it had obtained its strontium and fluorite from igneous rocks. Harder (pers. commun., 1993, cited in Symons, 1994) used fission track dating to obtain a Jurassic-Cretaceous age of 135.7±4.5 Ma to 140.6±4.7 Ma for fluorite from the Cave-in-Rock subdistrict. The true age of fluorite may be significantly greater, however, as the annealing temperature of fluorite is only 108 °C (Harder, 1986), which could have been reached without necessarily high burial depths or amounts of other forms of heating. Chesley et al. (1994) obtained a Permian age of 272±17 Ma for Cave-in-Rock fluorite using Sm-Nd method, which is consistent with the Permian age of igneous intrusive rocks in the district obtained by Zartman et al. (1967) and Snee and Hayes (1992). Paleomagnetic dating has been attempted by Symons (1994). His study showed Mississippian limestones outside of the Illinois-Kentucky district to have a mid-Pennsylvanian magnetization typical of Paleozoic limestones in the mid-continent, and probably a product of regional hydrothermal fluid flow induced by the Alleghanian-Ouachita orogeny.

However within the Illinois-Kentucky district itself, Symons (1994) found evidence of a Jurassic remagnetization that he interpreted to be associated with mineralization.

Fluid Inclusions

Fluid Inclusions are generally abundant in hydrothermal minerals from the Illinois-Kentucky district, particularly in fluorite. Hall and Freidman (1963) have estimated that fluorite from the Cave-in-Rock subdistrict can contain between 0.01 and 0.1 wt% inclusion fluid. Primary fluid inclusions are often intermixed within a dense tapestry of pseudosecondary and secondary fluid inclusions. Four types of fluid inclusions have been recognized in the district (Figure 3; Richardson and Pinckney, 1984). Type I fluid inclusions constitute the majority and consist of an aqueous liquid and vapor phase. They can be primary, secondary, or pseudosecondary in origin and occur in all of the hydrothermal minerals. Fluid inclusions containing hydrocarbons are also abundant. Type II fluid inclusions consist of oil and a vapor-phase. The oil is typically yellow or brown in color and commonly contains dark spots of bitumen or degraded organic matter. Type II inclusions are typically round or oval in shape and primary in origin. Type III fluid inclusions consist of an aqueous liquid, vapor, and liquid oil phase. Most are secondary or pseudosecondary in origin but some are primary. They are most common in fluorite but also occur in quartz and calcite. Type IV fluid inclusions, which consist of aqueous liquid, vapor, and a daughter mineral were not observed in the present study.

Microthermometry

In order to be able to convert atomic ratios determined from LA-ICP-MS analysis of fluid inclusions to absolute concentrations and to look for correlations between fluid composition and temperature, microthermometry was first performed on the fluid inclusions. With the exception of the Hastie Quarry, no mining was occurring in the district at the time of this study so that sampling of in situ mineralization was generally not possible. Most of the samples for this study were collected from ore waste piles adjacent to abandoned mine shafts. Additional samples of in

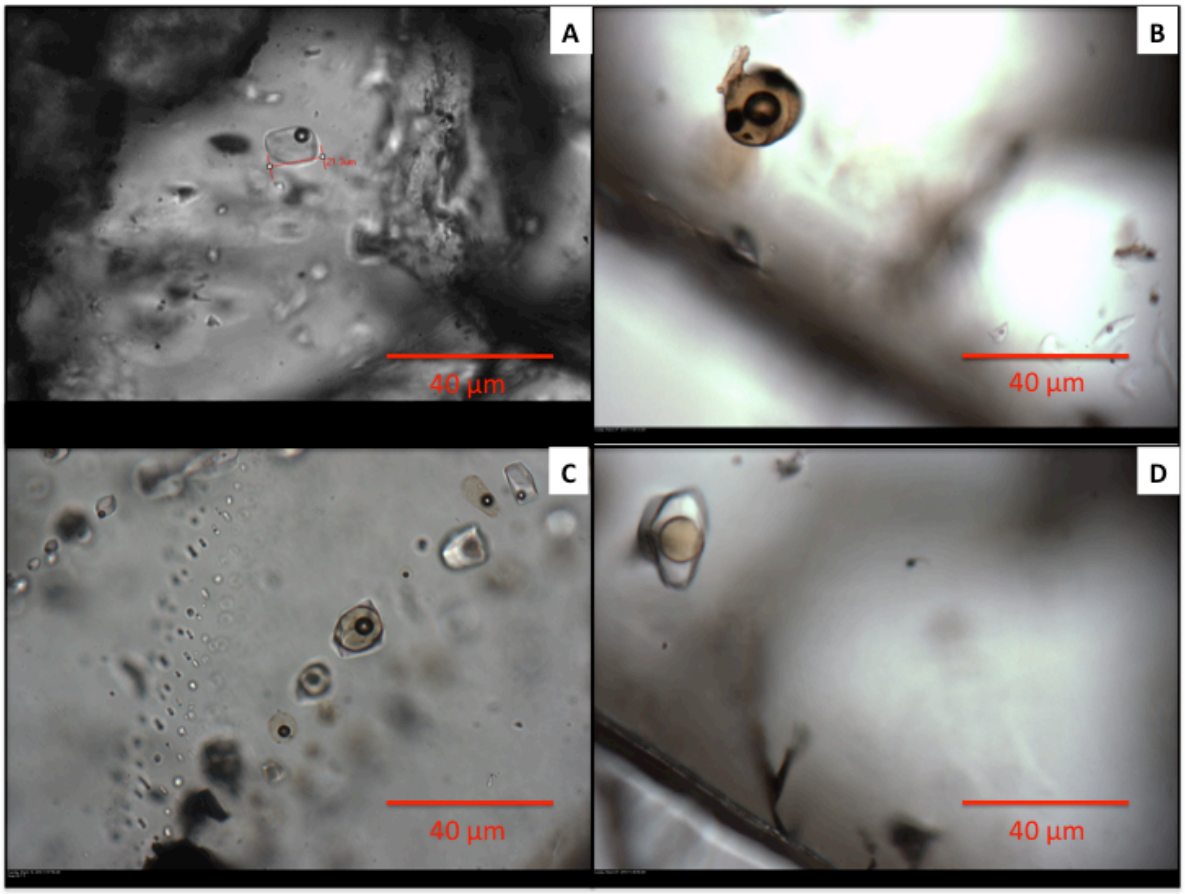

Figure 3: Photomicrographs of fluid inclusion types observed in the present study. (a) Type I, (b) Type II, (c) and (d) Type III.

situ mineralization were obtained from Dr. Paul Spry of Iowa State University, Ross Lillie of North Star Minerals, and Ray Guillemette of the Illinois State Geological Survey. A complete list of the names and locations of the deposits analyzed in this study is shown in Table 1.

Samples were prepared as doubly polished thin sections between 120-180 μm thick. To prevent fluid inclusions from stretching during polishing, a low temperature was maintained by using water as the polishing lubricant. Petrographic analysis was carried out in accordance with the paragenetic classifications of Richardson and Pinckney (1984), and primary inclusion origin was determined based on the criteria of Goldstein and Reynolds (1994). Despite the common presence of clearly defined growth features, identifying primary fluid inclusions was often hampered by the presence of dense planes of psuedosecondary and secondary inclusions that intersected the primary fluid inclusion assemblages. Upon the conclusion of the petrographic analysis, microthermometry was performed on the identified primary assemblages.

Microthermometry was performed using a Linkam THGMS 600 heating and cooling stage at the University of Missouri—Columbia. For every sample chip the homogenization temperatures of all the fluid inclusions were always measured before their last-ice-melting temperatures so that any stretching of the fluid inclusions during freezing would not lead to errors in the homogenization temperature measurement. Last ice melting temperatures were measured progressively on fluid inclusions with the lowest to the highest homogenization temperatures. To overcome kinetic inhibitions to freezing caused by high salinity, each fluid inclusion was super-cooled to a temperature between −59.0 and −70.0 °C. Last ice melting temperatures were converted to eq. wt% NaCl using the equation of state of Bodnar (1993) for a H_2O-NaCl solution. The standard deviation for measured fluid inclusion assemblages was ±1.3 °C for homogenization temperatures and ±0.09 °C for last-ice-melting temperature.

Results

A total of 160 fluid inclusions hosted by fluorite, calcite, sphalerite, and quartz were

Name	Sample ID	UTM
Hastie Quarry	IKHC	0606069 4151017
Hill Mine	IKHL	0396455 4156051
Minerva Mine	IKMV	0397910 4155678
Oxford Mine	IKOX	0396879 4154792
North Green Mine	IKNG	0396396 4153779

Table 1: Locations and identification codes of deposits analyzed in the present study. The reference datum used was World Geodetic Survey 1984 (WGS 84).

analyzed by microthermometry. The results of microthermometry are shown in Table 2. Figure 4 shows the homogenization temperature range of primary fluid inclusions hosted by minerals at different stages of the paragenesis, including data from the present study and from the studies by Richardson and Pinckney (1984) and Fuhrmann (1994). Homogenization temperatures vary mainly between about 100 and 150° C for most of the paragenesis until the deposition of late calcite during Episode IV. The wide variability in the homogenization temperatures may be due to the relative softness of the host minerals, making their fluid inclusions susceptible to variable post-entrapment stretching. Some of the discrepancies between the homogenization temperatures obtained in the present study and those obtained in previous studies may also be due to this stretching and that for many paragenetic stages only relatively small numbers of fluid inclusions are being compared.

Figure 5 shows fluid inclusion salinity as a function of paragenesis. The results are generally consistent with those obtained by previous researchers. Median salinities increase during episode II from about 15.5 eq. wt% NaCl in fluid inclusions in Y1 fluorite to around 21 eq. wt% NaCl in the fluid inclusions in Y2 fluorite. During the remainder of episode II and early part of episode III, median salinites fluctuate between 19 and 22 eq. wt% NaCl with the exception of some calcite-hosted fluid inclusions measured by Richards and Pinckney (1984) that have a median salinity of about 5.5 eq. wt% NaCl and may actually be secondary in origin. From P3 fluorite deposition in episode III to late calcite deposition in episode IV, median fluid inclusion salinities decrease steadily from about 20.5 to 22 eq. wt% NaCl to about 3 to 7.5 eq. wt% NaCl. This salinity pattern could represent the displacement of a resident brine by a more saline incoming brine that was in turn displaced by a dilute, possibly meteoric fluid. Such a pattern is consistent with numerical models for topographically driven groundwater flow that is often associated with the Ouachita orogeny, in which deep sedimentary brines in the Arkoma foreland basin are driven into stratigraphically shallower levels of the platform before being diluted by

Table 2: List of fluid inclusion microthermometry measurements.

Sample ID	Incl. ID	Paragenetic Phase	Size (µm)	Th (°C)	Ice Melting (°C)	Salinity (eq. wt% NaCl)
IKHL2-1	1A	Calcite	8.6x7.7	94.0	-13.8	17.6
IKHL2-1	1B	Calcite	12.7x10.5	133.2	-15.9	19.4
IKHL2-1	1C	Calcite	7.4x7.3	140.2	-19.9	22.4
IKHL2-1	2A	Calcite	9.8x9.0	114.4	-15.1	18.7
IKHL2-1	3A	Calcite	12.6x10.3	116.7	-17.2	20.4
IKHL2-1	3B	Calcite	8.6x8.6	117.4	-17.1	20.4
IKHL2-1	4A	Calcite	10.7x9.9	121.4	-	-
IKHL2-1	5A	Calcite	17.5x12.7	126.3	-13.3	17.2
IKHL2-1	5B	Calcite	11.2x7.3	148.7	-13.8	17.6
IKHL2-1	5C	Calcite	9.0x5.1	-	-18.5	21.4
IKHL2-1	6A	Calcite	8.5x4.9	131.7	-15.2	18.8
IKHL2-1	6B	Calcite	15.3x3.1	135.9	-15.2	18.8
IKHL2-1	7A	Calcite	7.6x5.3	162.3	-21.5	23.5
IKHL2-1	8A	Calcite	25.3x23.0	176.9	-15.0	18.6
IKHL2-1	9A	Calcite	40.5x15.3	140.2	-14.0	17.8
IKHL2-1	9B	Calcite	12.5x12.4	116.7	-14.2	18.0
LC1-1	7A	Late Calcite	19.4x16.0	74.4	-2.3	3.9
LC1-1	7B	Late Calcite	8.8x8.2	80.2	-1.9	3.2
LC1-1	7C	Late Calcite	42.4x13.4	89.1	-2.1	3.5
LC1-1	8A	Late Calcite	18.8x8.6	62.3	-1.5	2.5
LC1-1	8B	Late Calcite	19.2x10.1	-	-	-
LC1-1	8C	Late Calcite	12.9x10l0	62.1	-	-
LC1-1	8D	Late Calcite	14.0x8.2	-	-	-
IKHC1-12	2A	P1 Fluorite	54.7x38.9	120.1	-11.5	15.5
IKHC1-12	2B	P1 Fluorite	60.6x39.2	120.8	-10.3	14.2
IKHC1-12	2C	P1 Fluorite	183.5x140.1	-	-	-
IKHC1-12	2D	P1 Fluorite	63.6x60.0	119.3	-11.6	15.6
IKHC1-12	3A	P1 Fluorite	9.5x9.2	137.7	-17.6	20.7
IKHC1-12	3B	P1 Fluorite	8.5x8.4	146.4	-17.7	20.8
IKHC1-12	3C	P1 Fluorite	29.3x8.3	136.3	-9.0	12.9
IKHC1-12	6A	P1 Fluorite	8.2x6.5	126.5	-18.1	21.1
IKHC1-12	6B	P1 Fluorite	35.2x12.3	104.5	-4.9	7.7
IKHC1-12	6C	P1 Fluorite	12.3x9.7	119.3	-10.8	14.8
IKHC1-12	6D	P1 Fluorite	7.0x5.7	119.1	-18.0	21.0
IKHC1-12	6E	P1 Fluorite	39.4x33.8	126.3	-18.1	21.1
IKHL2-2	1A	P2 Fluorite	178.2x110.2	140.9	-15.2	18.8
IKHL2-2	1B	P2 Fluorite	98.7x88.8	137.6	-16.9	20.2
IKHL2-2	1C	P2 Fluorite	58.4x47.4	108.3	-	-
IKHL2-21	3A	P2 Fluorite	11.1x10.0	138.4	-16.8	20.1
IKHL2-21	3B	P2 Fluorite	17.2x13.3	139.6	-16.8	20.1
IKHL2-21	3C	P2 Fluorite	17.0x11.7	140.1	-16.8	20.1
IKHL2-21	6A	P2 Fluorite	27.6x6.3	116.9	-19.0	21.8
IKHL2-21	6B	P2 Fluorite	6.5x6,6	116.4	-18.6	21.5
IKHL2-21	6C	P2 Fluorite	25.1x6.6	116.8	-18.7	21.6
IKHL2-6	3A	P3 Fluorite	26.0x22.1	149.1	-19.0	21.7
IKHL2-6	3B	P3 Fluorite	35.4x28.6	162.1	-2.5	4.1
IKHL2-6	3C	P3 Fluorite	25.1x22.0	149.9	-19.2	21.9
IKHL2-6	5C	P3 Fluorite	13.0x13.7	140.7	-19.7	22.3
IKHL2-6	5B	P3 Fluorite	7.7x5.6	142.9	-19.9	22.4
IKHL2-6	5C	P3 Fluorite	9.9x7.9	136.7	-19.1	21.8
IKHL2-6	6A	P3 Fluorite	25.224.7	114.4	-	-
IKHL2-6	6B	P3 Fluorite	22.7x19.2	119.3	-	-
IKHL2-6	6C	P3 Fluorite	28.1x17.0	111.4	-	-

Sample ID	Incl. ID	Paragenetic Phase	Size (µm)	Th (°C)	Ice Melting (°C)	Salinity (eq. wt% NaCl)
IKNG1-7	1A	P3 Fluorite	10.9x8.5	105.8	-19.2	21.9
IKNG1-7	1B	P3 Fluorite	10.4x5.6	108.8	-19.2	21.9
IKNG1-7	1C	P3 Fluorite	9.1x7.8	114.4	-19.3	22.0
IKNG1-7	4A	P3 Fluorite	10.8x10.6	118.8	-19.2	21.9
IKNG1-7	4B	P3 Fluorite	12.1x12.0	121.7	-18.4	21.3
IKHL2-4	8A	P4 Fluorite	21.2x11.1	116.4	-12.3	16.3
IKHL2-4	8B	P4 Fluorite	13.8x12.9	123.5	-12.5	16.5
IKHL2-4	8C	P4 Fluorite	58.9x34.6	166.6	-12.3	16.3
IKHL2-4	8D	P4 Fluorite	18.7x6.3	121.6	-12.6	16.6
IKHL2-6	1A	P4 Fluorite	31.0x23.4	127.5	-16.9	20.2
IKHL2-6	1B	P4 Fluorite	12.3x12.1	140.2	-16.9	20.2
IKHL2-7	1A	P4 Fluorite	15.9x9.0	137.5	-18.3	21.3
IKHL2-7	1B	P4 Fluorite	17.27.5	138.2	-18.3	21.3
IKHL2-7	1C	P4 Fluorite	13.8x8.6	145.1	-17.0	20.2
IKHL2-7	2A	P4 Fluorite	56.9x55.1	144.8	-16.6	19.9
IKHL2-7	2B	P4 Fluorite	78.6x50.1	146.1	-16.6	19.9
IKHL2-7	2C	P4 Fluorite	55.0x48.1	146.2	-16.7	20.0
IKHL2-7	3A	P4 Fluorite	15.6x12.1	136.6	-16.5	19.9
IKHL2-7	3B	P4 Fluorite	5.7x4.0	139.3	-15.5	19.1
IKHL2-7	4A	P4 Fluorite	16.9x8.8	144.8	-16.9	20.2
IKHL2-7	4B	P4 Fluorite	13.3x7.2	143.3	-16.4	19.8
IKHL2-7	4C	P4 Fluorite	12.2x6.6	142.7	-16.5	19.9
IKHL2-7	4D	P4 Fluorite	13.2x9.8	145.7	-16.4	19.8
IKHL2-7	6A	P4 Fluorite	30.3x24.1	97.1	-	-
IKHL2-7	6B	P4 Fluorite	10.4x10.0	112.6	-	-
IKHL2-7	6C	P4 Fluorite	23.5x21.1	98.8	-	-
IKNG1-7	2A	P4 Fluorite	21.3x20.8	121.2	-18.1	21.1
IKNG1-7	2B	P4 Fluorite	41.712.5	123.1	-18.3	21.3
IKNG1-7	2C	P4 Fluorite	27.4x14.1	122.2	-18.4	21.3
IKNG1-7	3A	P4 Fluorite	45.2x37.6	130.0	-17.8	20.9
IKNG1-7	3B	P4 Fluorite	27.8x17.5	132.3	-17.9	21.0
IKHL2-4	1A	P5 Fluorite	43.0x35.4	144.9	-16.0	19.5
IKHL2-4	1B	P5 Fluorite	16.6x16.0	145.2	-16.0	19.5
IKHL2-4	1C	P5 Fluorite	23.3x17.5	144.4	-16.1	19.5
IKHL2-4	4A	P5 Fluorite	17.1x9.9	143.1	-16.8	20.1
IKHL2-4	4B	P5 Fluorite	11.8x8.5	141.7	-16.2	19.7
IKHL2-4	4C	P5 Fluorite	9.7x8.0	140.3	-16.5	19.9
IKHL2-4	5A	P5 Fluorite	19.2x12.1	144.1	-16.1	19.6
IKHL2-4	5B	P5 Fluorite	9.5x9.4	144.7	-16.0	19.5
IKHL2-4	5C	P5 Fluorite	11.4x10.1	151.4	-16.1	19.6
IKHL2-4	6B	P5 Fluorite	9.5x7.9	142.6	-15.1	18.8
IKHL2-4	3A	P6 Fluorite	10.7x8.5	137.0	-14.9	18.6
IKHL2-4	3B	P6 Fluorite	11.1x6.7	139.5	-14.4	18.2
IKHL2-4	3C	P6 Fluorite	8.1x7.9	133.7	-13.0	16.9
IKHL2-4	3D	P6 Fluorite	14.5x10.5	-	-15.1	18.7
IKHL2-4	5D	P6 Fluorite	9.9x7.8	141.8	-16.2	19.7
IKHL2-4	6A	P6 Fluorite	25.4x13.4	150.8	-13.9	17.7
IKHL2-4	6C	P6 Fluorite	23.1x14.7	143.1	-14.6	18.3
IKHL2-4	6D	P6 Fluorite	12.4x10.5	141.5	-14.1	17.9
IKHL2-4	2A	P7 Fluorite	17.4x13.1	126.4	-13.2	17.1
IKHL2-4	2B	P7 Fluorite	36.3x28.5	133.5	-12.4	16.3
IKHL2-4	2C	P7 Fluorite	13.9x12.6	128.9	-12.5	16.4
IKDM1-1	1A	Quartz	39.5x19.0	95.0	-17.1	20.4

Sample ID	Incl. ID	Paragenetic Phase	Size (μm)	Th (°C)	Ice Melting (°C)	Salinity (eq. wt% NaCl)
IKDM1-1	3A	Quartz	12.7x7.8	143.4	-18.5	21.4
IKHL1-3	1A	Sphalerite	28.3x22.0	116.3	-22.6	24.2
IKHL1-3	1B	Sphalerite	8.8x6.8	114.5	-22.5	24.2
IKHL1-3	2A	Sphalerite	11.5x6.8	114.4	-13.8	17.6
IKHL1-3	2B	Sphalerite	7.4x6.9	117.0	-14.1	17.9
IKHL1-3	2C	Sphalerite	21.5x20.1	117.4	-13.6	17.5
IKHL1-3	3A	Sphalerite	26.3x17.9	129.8	-17.6	20.7
IKHL1-3	4A	Sphalerite	15.8x21.8	130.7	-13.3	17.2
IKHL1-3	4B	Sphalerite	43.6x30.4	127.2	-13.4	17.2
IKHL1-3	4C	Sphalerite	17.5x14.7	127.0	-13.4	17.2
IKHL1-3	5A	Sphalerite	16.6x15.9	136.5	-20.0	22.4
IKHL1-3	5B	Sphalerite	9.8x8.5	-	-19.8	22.3
IKHL1-3	6A	Sphalerite	30.8x12.5	122.8	-21.3	23.4
IKHL1-3	6B	Sphalerite	13.4x7.9	-	-20.2	22.6
IKHL1-3	6C	Sphalerite	42.6x29.6	120.1	-19.7	22.3
IKHL1-3	6D	Sphalerite	13.3x12.2	120.3	-19.9	22.4
IKHL1-3	11A	Sphalerite	25.9x9.2	103.4	-13.9	17.7
IKHL1-3	11B	Sphalerite	8.8x9.0	103.3	-12.7	16.6
IKHL1-3	11C	Sphalerite	22.4x8.9	102.5	-12.7	16.6
IKHL1-3	11D	Sphalerite	24.4x8.9	101.3	-12.3	16.3
IKHL1-3	13A	Sphalerite	24.4x16.4	127.7	-20.7	23.0
IKHL1-3	13B	Sphalerite	16.2x9.1	12.8	-20.7	23.0
IKHL1-3	13C	Sphalerite	13.7x13.0	126.9	-21.3	23.4
IKHL2-9	1A	Sphalerite	29.7x19.9	121.7	-20.0	22.5
IKHL2-9	1B	Sphalerite	15.9x13.3	121.7	-20.7	22.9
IKHL2-9	2A	Sphalerite	18.5x15.0	123.4	-19.8	22.3
IKMV1-4	1A	Sphalerite	15.2x11.8	106.9	-20.6	22.9
IKMV1-4	1B	Sphalerite	6.5x6.5	114.3	-20.0	22.5
IKMV1-4	3A	Sphalerite	16.5x8.9	115.0	-16.3	19.7
IKMV1-4	3B	Sphalerite	20.6x18.3	116.1	-13.0	16.9
IKMV1-4	3C	Sphalerite	19.9x8.1	110.6	-13.3	17.2
IKMV1-4	3D	Sphalerite	34.0x19.2	118.4	-13.4	17.3
IKMV1-4	4A	Sphalerite	15.3x9.1	135.6	-18.5	21.4
IKMV1-4	4B	Sphalerite	22.8x8.9	119.3	-18.7	21.6
IKMV1-4	4C	Sphalerite	19.5x13.6	118.5	-18.5	21.4
IKMV1-4	4D	Sphalerite	22.8x5.0	118.5	-18.6	21.5
IKMV2-12	2A	Sphalerite	18.7x14.4	-	-20.7	23.0
IKHC1-12	1A	Y1 Fluorite	47.1x38.6	123.5	-10.2	14.1
IKHC1-12	1B	Y1 Fluorite	36.8x33.5	142.8	-13.7	17.6
IKHL2-21	1A	Y2 Fluorite	122.1x110.4	121.2	-	-
IKHL2-21	1B	Y2 Fluorite	143.7x133.0	123.3	-17.6	20.7
IKHL2-21	5A	Y2 Fluorite	25.1x14.4	130.7	-13.2	17.1
IKHL2-21	5B	Y2 Fluorite	15.1x10.3	130.7	-13.1	17.0
IKHL2-21	5C	Y2 Fluorite	19.9x14.3	131.9	-13.0	16.9
IKHL2-5	1A	Y2 Fluorite	21.0x19.0	118.9	-	-
IKHL2-5	1B	Y2 Fluorite	44.1x27.9	120.5	-18.3	21.3
IKHL2-5	1C	Y2 Fluorite	34.9x32.5	131.6	-18.5	21.4
IKHL2-5	2A	Y2 Fluorite	26.0x22.0	142.8	-16.2	19.7
IKHL2-5	2B	Y2 Fluorite	21.0x17.9	129.2	-17.0	20.2
IKHL2-5	3A	Y2 Fluorite	29.5x8.3	97.5	-18.8	21.6
IKHL2-5	3B	Y2 Fluorite	13.7x12.4	101.3	-18.6	21.5
IKHL2-5	3C	Y2 Fluorite	12.3x9.2	121.9	-18.7	21.6
IKHL2-5	4A	Y2 Fluorite	30.7x13.0	107.7	-16.8	20.1
IKHL2-5	4B	Y2 Fluorite	9.7x9.1	112.4	-18.6	21.5

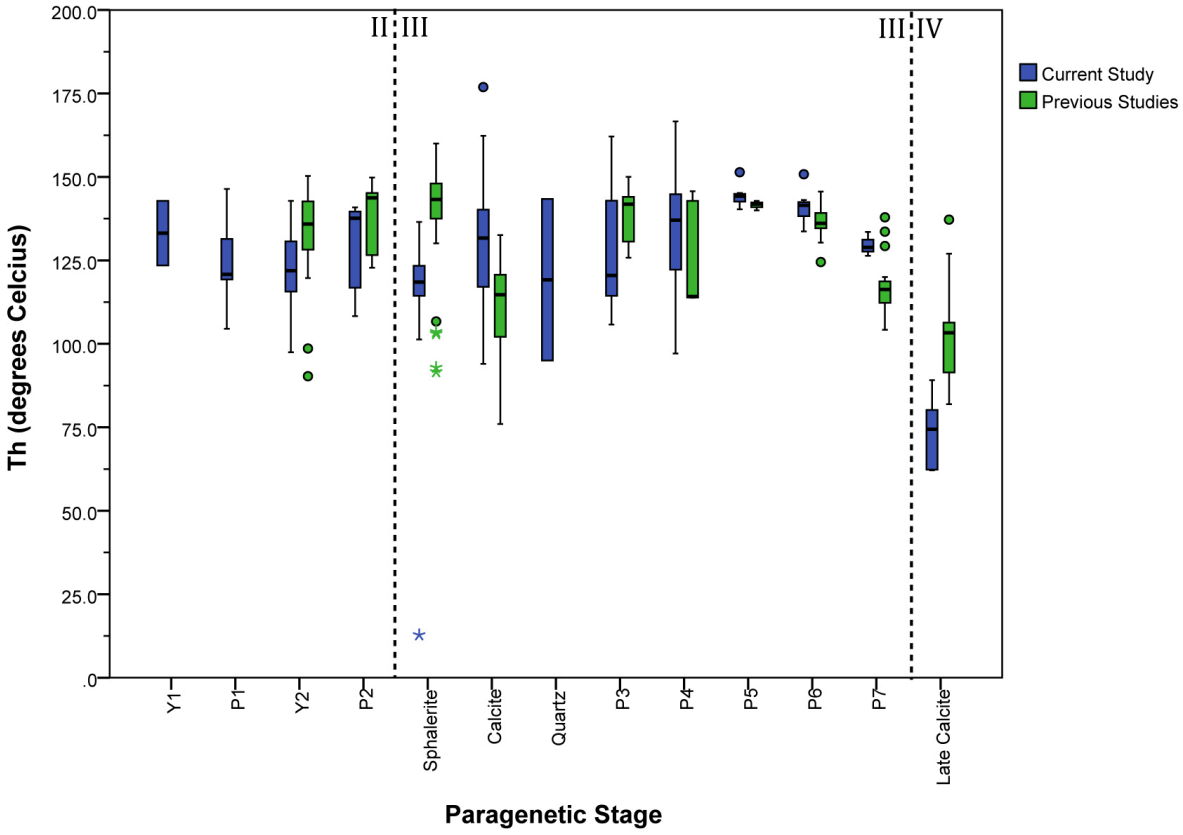

Figure 4: Box-plot of homogenization temperatures of primary fluid inclusions from the Cave-in-Rock subdistrict as a function of paragenetic stage. Plot includes data from the present study and from Richardson and Pinckney (1984), and Fuhrmann (1994). The dashed lines here and in subsequent figures containing plots of a parameter as a function of paragenesis represent the boundaries between discrete paragenetic episodes described in the text. Here and in succeeding figures containing box plots, the upper and lower portions of the boxes represent the 75th and 25th percentile, and the whiskers represents the highest and lowest values that are not outliers.

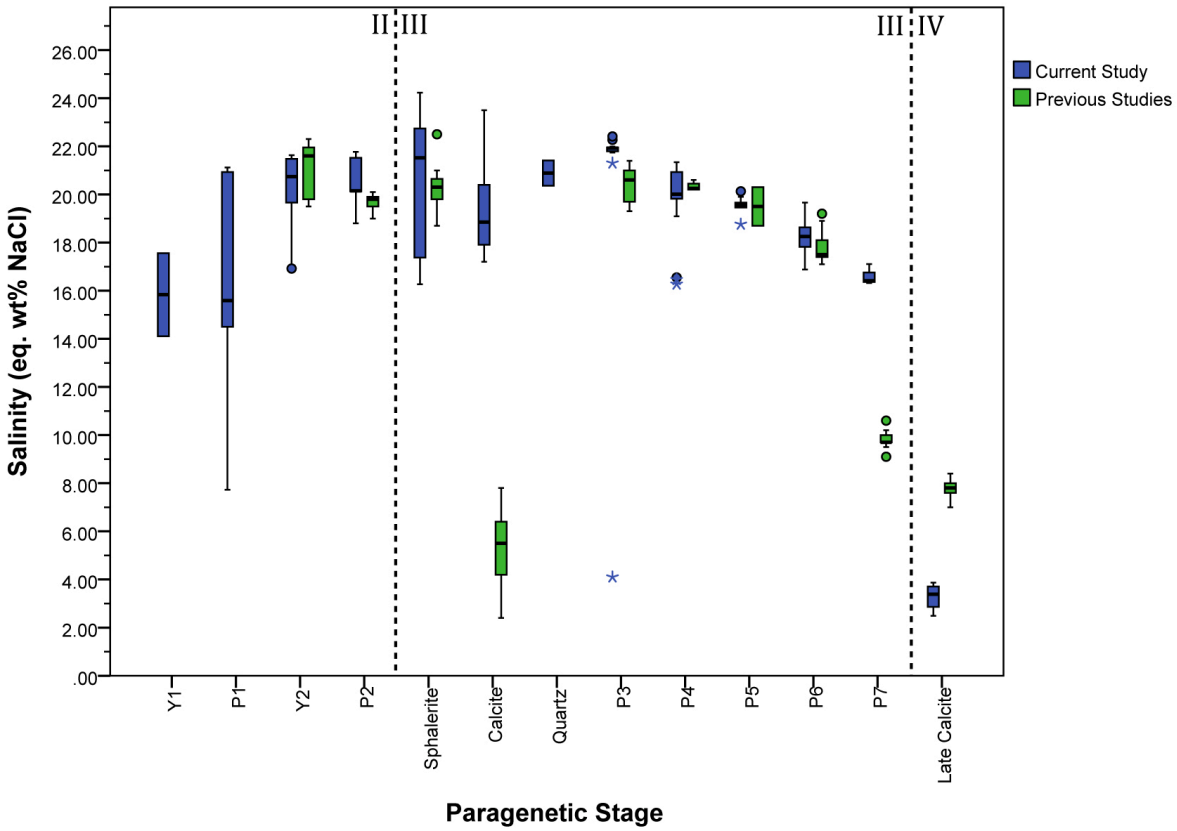

Figure 5: Box-plot of fluid inclusion salinity as a function of paragenetic stage determined in the present study and by Richardson and Pinckney (1984) and Fuhrmann (1994).

meteoric recharge (Garven et al., 1993; Appold and Garven, 1999; Appold and Nunn, 2005).

When fluid inclusion salinity is plotted versus homogenization temperature at least three discrete populations are visible (Figure 6). Population A consists of the most saline inclusions and has a slight negative slope. Population B consists of fluid inclusions with intermediate salinities, a similar homogenization temperature range to population A, and a slight positive slope. Population C consists of cool and dilute fluid inclusions from episode IV calcite, whereas populations A and B consist of fluid inclusions from episodes II and III. Fuhrman (1994) and Spry and Fuhrman (1994) recognized similar trends in their microthermometry data, and interpreted the trends to be the result of mixing among three fluids: a lower temperature-higher salinity brine (F1: <125 °C, 23 eq. wt% NaCl), a higher temperature-lower salinity brine (F2: ~150 °C, 19 eq. wt% NaCl), and a lower temperature-lower salinity meteoric-dominated fluid (F3: <125 °C, <10 eq. wt% NaCl).

LA-ICP-MS Analysis

Upon the completion of the microthermometry, the elemental concentrations of fluid inclusions were measured using an Agilent 7500ce quadrupole ICP-MS coupled to a GeolasPro Excimer 193-nm ArF laser ablation system housed at the Virginia Polytechnical Institute and State University in Blacksburg, VA. The instrument was calibrated utilizing the NIST610 glass standard, which was analyzed at regular intervals during each analytical session to account for instrument drift. Samples were ablated in a 1.5 cm^3 ablation cell using a laser output energy of 150 mJ. Beam size was adjusted based on the size of the fluid inclusion in order to ablate each inclusion fully. Ablated material was transported from the ablation cell by He gas flowing at a rate of 0.7 mL min^{-1}. The analyte was then mixed with 1.03 L min^{-1} Ar gas before introduction into the plasma. The ICP-MS was operated at an RF power of 1500 W with a dwell time per isotope of 10 ms. Reduction of the raw LA-ICP-MS data was done using the ExLAM software (Zacharias and Wilkinson, 2007) using Na as the internal standard. ExLAM was used in order to

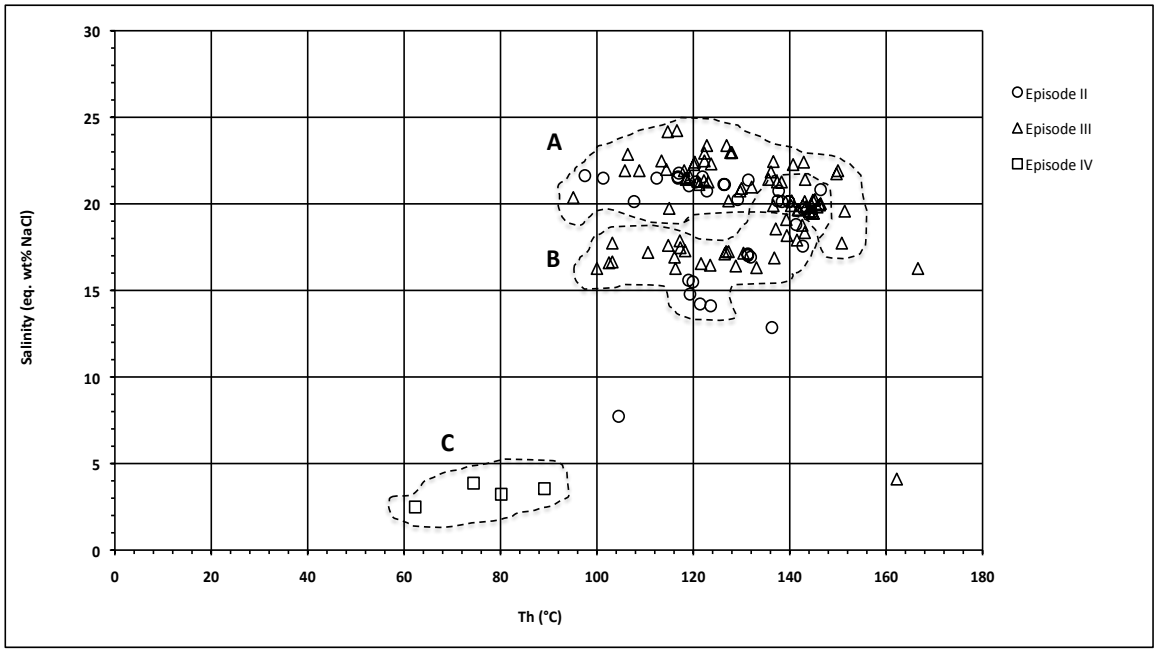

Figure 6: Fluid inclusion salinity versus homogenization temperature for analyses from the present study. Discrete fluid inclusion populations are outline by dashed lines.

take advantage of its ability to treat fluid inclusions that contains isotopes present in both the fluid and the mineral matrix. The Na concentration in the fluid inclusions was obtained independently from the last ice-melting temperature, which was converted to equivalent weight percent NaCl.

Results

Fluid inclusions hosted in fluorite, sphalerite, and calcite were analyzed to determine their elemental concentrations of Li, Na, Mg, Si, K, Ca, Mn, Fe, Cu, Zn, As, Rb, Sr, Ag, Cd, Ba, and Pb. Absolute elemental ppm for sphalerite-hosted fluid inclusions are displayed in Table 3 and atomic ratios for sphalerite-, fluorite-, and calcite-hosted fluid inclusions are displayed in Table 4. Absolute elemental concentrations could not be calculated for fluorite- or calcite-hosted fluid inclusions because the equation of Heinrich et al. (2003) that relates equivalent weight percent NaCl to the sum of the major chloride species concentrations in solution could not be used as the aqueous Ca signal was not quantifiable because of interference from the host mineral matrix. Thus, for fluorite- and calcite-hosted fluid inclusions, only atomic ratios could be determine. In sphalerite-hosted inclusions and Zn and Cd were not quantifiable because of interferences from high concentrations of these elements in the host mineral matrix. However, the contribution of these elements to the total salinity of the fluid inclusions is small enough so that the Heinrich et al. (2003) equation could be used to calculate absolute concentrations of other elements. The elements Li, Si, Mn, As, Rb, and Ag were not abundant in the matrices of any of the host minerals studied but generally did not exist in detectable concentrations in any fluid inclusions either. The relative standard deviation (RSD) for atomic ratios of fluid inclusion assemblages for the most reliably detected elements varied from 6 to 44% for K/Na, 10 to 33% for Ca/Na, 7 to 44% for Mg/Na, 10 to 52% for Ca/Mg, and 11 to 42% for Sr/Na. The minor elements and metals that were detected successfully within fluid inclusion assemblages had much higher RSD values, Ba/Na and Pb/Na RSD varied from 9 to 66% and 42 to 65% respectively. Zn/Na, Cu/Na, and Fe/Na atomic ratios were not quantifiable within multiple fluid inclusions within any fluid inclusion assemblages.

Sample ID	Paragenetic Phase	23Na	25Mg	39K	40Ca	56Fe	63Cu	66Zn	88Sr	138Ba	208Pb
IKHL2-9	Sphalerite	6.4E+04	1.1E+03	4.2E+03	1.7E+04	-	-	-	1.2E+03	3.9E+01	-
IKHL2-9	Sphalerite	6.0E+04	1.6E+03	3.5E+03	2.0E+04	-	-	-	1.4E+03	4.2E+01	-
IKHL1-3	Sphalerite	7.2E+04	-	-	2.1E+04	-	-	-	1.6E+03	4.8E+01	-
IKHL1-3	Sphalerite	6.5E+04	-	-	1.5E+04	-	-	-	3.8E+02	-	-
IKHL1-3	Sphalerite	6.0E+04	-	-	7.1E+03	-	-	-	5.1E+02	1.6E+01	-
IKHL1-3	Sphalerite	5.8E+04	1.4E+03	3.9E+03	2.2E+04	-	-	-	1.4E+03	6.1E+01	-
IKHL1-3	Sphalerite	5.4E+04	1.0E+03	-	9.6E+03	-	-	-	6.2E+02	1.3E+01	-
IKHL1-3	Sphalerite	6.2E+04	9.6E+02	4.8E+03	1.9E+04	-	-	-	1.1E+03	6.6E+01	-
IKHL2-9	Sphalerite	8.2E+04	-	-	7.3E+03	-	-	-	5.2E+02	3.5E+01	-
IKHL2-9	Sphalerite	6.4E+04	1.3E+03	3.5E+03	1.7E+04	-	-	-	8.1E+02	3.9E+01	-
IKHL1-3	Sphalerite	5.6E+04	8.9E+02	-	1.9E+04	-	-	-	1.1E+03	5.1E+01	-
IKHL1-3	Sphalerite	6.1E+04	-	-	2.3E+04	-	-	-	1.6E+03	1.0E+02	-
IKHL1-3	Sphalerite	5.6E+04	5.3E+02	-	8.7E+03	-	-	-	6.6E+02	9.1E+00	-
IKHL1-3	Sphalerite	6.2E+04	9.6E+02	5.0E+03	1.8E+04	-	-	-	1.1E+03	6.2E+01	-
IKMV1-4	Sphalerite	6.3E+04	1.2E+03	2.3E+03	1.9E+04	-	-	-	1.4E+03	-	-
IKMV1-4	Sphalerite	8.3E+04	-	-	-	-	-	-	2.0E+03	6.3E+01	-
IKMV1-4	Sphalerite	5.7E+04	6.8E+02	-	2.1E+04	-	-	-	1.5E+03	7.8E+01	-
IKHL1-3-3B	Sphalerite	7.2E+04	-	3.8E+03	6.0E+03	-	-	-	3.9E+02	1.1E+01	-
IKHL1-3-3C	Sphalerite	5.9E+04	1.0E+03	3.7E+03	1.6E+04	-	-	-	1.1E+03	4.4E+01	-
IKHL1-3-3D	Sphalerite	5.7E+04	1.1E+03	3.7E+03	1.7E+04	-	-	-	1.2E+03	3.6E+01	-
IKHL1-3-3E	Sphalerite	5.7E+04	8.0E+02	2.8E+03	1.8E+04	-	-	-	1.3E+03	-	1.8E+02
IKHL1-3-3F	Sphalerite	5.5E+04	1.2E+03	3.3E+03	2.0E+04	-	-	-	1.2E+03	3.6E+01	-
IKMV2-12-2A	Sphalerite	6.8E+04	1.1E+03	1.7E+03	1.7E+04	-	-	-	1.3E+03	3.1E+01	-
IKMV2-12-2B	Sphalerite	6.5E+04	1.2E+03	1.9E+03	1.9E+04	-	-	-	1.4E+03	2.1E+01	4.0E+01
IKMV2-12-2C	Sphalerite	7.2E+04	-	-	1.6E+04	-	-	-	1.2E+03	2.3E+01	-
IKMV2-12-2D	Sphalerite	6.6E+04	1.3E+03	2.5E+03	1.8E+04	-	-	-	1.2E+03	2.5E+01	-

Table 3: LA-ICP-MS results from sphalerite-hosted fluid inclusions.

Sample ID	Paragenetic Phase	Mg/Na	K/Na	Ca/Na	Ca/Mg	Fe/Na	Cu/Na	Zn/Na	Sr/Na	Ba/Na	Pb/Na
IKHL2-1-1A	Calcite	-	2.2E-02	-	-	-	-	-	-	-	5.8E-05
IKHL2-1-2A	Calcite	-	8.1E-02	-	-	-	-	-	-	1.1E-04	6.3E-04
IKHL2-1-2B	Calcite	1.3E-01	4.9E-02	-	-	1.2E-02	-	-	1.5E-02	4.4E-03	2.7E-04
IKHL2-1-3A	Calcite	-	1.8E-02	-	-	-	-	-	-	4.8E-04	-
IKHL2-1-3B	Calcite	-	2.7E-02	-	-	-	-	-	6.7E-03	1.8E-04	-
IKHL2-1-5A	Calcite	1.7E-02	5.4E-02	-	-	-	-	-	1.0E-02	6.1E-05	-
IKHL2-1-5B	Calcite	4.8E-02	3.7E-02	-	-	-	-	-	5.5E-03	2.8E-05	-
IKHL2-1-6B	Calcite	1.5E-02	2.5E-02	-	-	-	-	-	4.3E-03	1.4E-04	-
IKHL2-1-7A	Calcite	-	3.0E-02	-	-	-	-	-	1.5E-02	6.1E-04	4.6E-04
IKHL2-1-7C	Calcite	7.1E-02	1.6E-02	-	-	-	-	-	3.9E-03	2.1E-05	-
IKHC1-12	Y1	5.0E-03	2.6E-02	-	-	1.2E-04	3.9E-04		2.4E-03	7.0E-05	-
IKHC1-12	P1	8.5E-03	2.7E-02	-	-		-	-	1.9E-03	2.9E-05	-
IKHC1-12	P1	2.2E-03	2.8E-02	-	-	2.6E-05	-	-	6.6E-04	-	-
IKHC1-12-6B	P1	-	-	-	-	6.4E-02	-	-	-	-	-
IKHC1-12-6C	P1	1.7E-02	4.8E-02	-	-	5.8E-05	-	-	5.2E-03	2.1E-04	-
IKHC1-12-6D	P1	1.5E-02	4.3E-02	-	-		1.1E-03		5.2E-03	2.4E-04	-
IKHL2-5	Y2	1.6E-02	4.1E-02	-	-	6.3E-04	6.1E-03		8.8E-04	4.0E-04	1.7E-04
IKHL2-5	Y2	-	1.9E-02	-	-	-	-	-	-	1.2E-05	-
IKHL2-21	Y2	1.4E-02	2.6E-02	-	-	-	-	-	4.5E-03	3.2E-05	-
IKHL2-5	Y2	-	4.5E-02	-	-	-	-	-	-	4.3E-05	-
IKHL2-21	Y2	5.4E-02	6.3E-02	-	-	5.0E-04	1.3E-05	2.7E-05	1.6E-02	1.7E-04	6.6E-05
IKHL2-5	Y2	3.3E-02	3.6E-02	-	-	2.9E-03		1.2E-02	2.0E-03	7.6E-04	6.2E-04
IKHL2-5-4A	Y2	1.8E-01	3.3E-02	-	-	-	-	-	2.9E-03	9.5E-04	-
IKHL2-5-4B	Y2	-	1.0E-01	-	-	-	-	-	-	-	-
IKHL2-2	P2	1.8E-02	4.2E-02	-	-	-	-	-	5.3E-03	1.9E-04	-
IKHL2-21	P2	1.4E-02	2.3E-02	-	-	-	-	-	5.8E-03	1.6E-03	-
IKHL2-21	P2	2.0E-01	9.9E-02	-	-	-	-	-	5.4E-03	-	-
IKHL2-21-6D	P2	1.5E-02	4.5E-02	-	-	1.1E-04	-		4.8E-03	1.9E-04	-
IKHL2-21-3A	P2	1.1E-02	5.0E-02	-	-	2.2E-04	-	2.3E-03	4.8E-03	-	-
IKHL2-6	P3	3.4E+00	4.1E-01	-	-	-	-	-	3.1E-02	8.7E-03	-
IKHL2-6	P3	2.3E+00	2.4E-01	-	-	-	-	-	3.9E-02	1.2E-02	-
IKHL2-6	P3	2.4E+00	4.2E-01	-	-	-	-	-	4.6E-02	6.2E-03	-
IKHL2-6-6A	P3	1.5E-02	2.7E-02	-	-	1.1E-03	1.2E-02	1.7E-03	3.1E-03	2.3E-04	1.8E-03
IKHL2-6-6B	P3	8.8E-03	4.0E-02	-	-	2.2E-03	5.0E-03	-	1.8E-03	4.5E-04	3.3E-03
IKHL2-6-6D	P3	-	3.4E-02	-	-	-	-	-	2.5E-03	-	-
IKHL2-6-6E	P3	-	-	-	-	-	-	-	-	-	-
IKNG1-7-1A	P3	5.7E-03	7.8E-03	-	-	-	-	-	5.7E-03	-	-
IKNG1-7-4B	P3	3.9E-02	5.7E-02	-	-	-	3.4E-03	6.2E-04	4.4E-03	6.4E-05	9.0E-05
IKNG1-7-4C	P3	2.8E-02	5.8E-02	-	-	-	-	-	6.0E-03	-	4.5E-06
IKHL2-7	P4	-	7.1E-02	-	-	1.9E-03	2.8E-02	7.9E-03	4.4E-03	3.7E-04	7.2E-04
IKHL2-7	P4	5.2E-01	1.6E-01	-	-	2.8E-02	1.2E-02	-	1.2E-02	3.8E-02	3.8E-03
IKHL2-7	P4	3.0E-02	3.6E-02	-	-	5.7E-04	2.7E-02	9.1E-03	6.4E-03	1.8E-04	1.2E-03
IKHL2-7	P4	4.1E-03	5.2E-02	-	-	-	3.4E-04	-	2.1E-03	1.4E-04	1.7E-06
IKHL2-7	P4	2.8E-01	2.2E-01	-	-	-	-	-	1.1E-02	5.1E-03	1.9E-02
IKHL2-7	P4	8.1E-01	-	-	-	-	-	-	-	8.4E-03	2.8E-02
IKHL2-7-3C	P4	2.9E-02	4.0E-02	-	-	2.3E-03	3.0E-02	2.3E-02	-	2.0E-04	4.1E-04
IKHL2-7-3E	P4	1.0E-02	1.3E-02	-	-	1.3E-04	5.2E-05	6.3E-04	1.1E-03	7.9E-05	2.4E-05
IKHL2-7-4A	P4	1.1E-03	1.2E-01	-	-	-	-	-	3.0E-04	9.8E-05	-
IKNG1-7-2A	P4	4.5E-02	2.8E-02	-	-	-	1.2E-04	9.9E-04	5.7E-03	2.7E-04	-
IKNG1-7-2B	P4	4.4E-03	5.6E-02	-	-	-	-	-	2.3E-04	4.7E-05	-
IKNG1-7-2C	P4	9.8E-03	4.3E-02	-	-	-	-	-	1.5E-03	1.2E-04	-
IKNG1-7-2D	P4	1.2E-02	3.6E-02	-	-	-	-	-	4.8E-03	1.2E-04	-
IKNG1-7-2E	P4	2.6E-02	2.8E-02	-	-	1.1E-02	1.1E-03	-	4.4E-03	4.6E-05	3.5E-05
IKNG1-7-3B	P4	2.9E-02	7.0E-02	-	-	-	-	-	7.9E-03	7.9E-05	-
IKNG1-7-3C	P4	9.8E-02	8.8E-02	-	-	8.0E-02	9.7E-03	4.1E-02	1.3E-02	1.7E-03	3.9E-04
IKHL2-4-4A	P5	-	-	-	-	-	-	-	-	-	-
IKHL2-4-5A	P5	7.1E-02	8.9E-02	-	-	-	-	-	5.3E-03	3.8E-04	-
IKHL2-4-6B	P5	3.4E-01	7.5E-02	-	-	-	-	-	7.1E-04	1.5E-03	-
IKHL2-4-2A	P7	1.8E-01	8.5E-02	-	-	7.1E-03	8.1E-03	1.6E-02	1.2E-03	3.9E-04	6.7E-03
IKHL2-4-2D	P7	5.2E-02	7.6E-02	-	-	-	-	-	6.3E-03	3.9E-04	-
IKHL2-9	Sphalerite	1.6E-02	3.8E-02	1.3E-01	8.3E+00	-	-	-	4.8E-03	1.0E-04	-
IKHL2-9	Sphalerite	2.5E-02	3.4E-02	1.7E-01	6.7E+00	-	-	-	6.3E-03	1.2E-04	-
IKHL1-3	Sphalerite	1.0E-02	1.6E-02	1.5E-01	1.4E+01	-	-	-	5.9E-03	1.2E-04	-
IKHL1-3	Sphalerite	-	3.5E-02	1.2E-01	-	-	-	-	1.5E-03	-	-
IKHL1-3	Sphalerite	8.9E-03	1.6E-02	6.1E-02	6.8E+00	-	-	-	2.2E-03	4.7E-05	-
IKHL1-3	Sphalerite	2.2E-02	3.9E-02	1.9E-01	8.8E+00	-	-	-	6.5E-03	1.8E-04	-
IKHL1-3	Sphalerite	1.8E-02	1.4E-02	9.1E-02	5.1E+00	-	-	-	3.0E-03	4.0E-05	-
IKHL1-3	Sphalerite	1.5E-02	4.6E-02	1.6E-01	1.1E+01	-	-	-	4.8E-03	1.9E-04	-
IKHL2-9	Sphalerite	-	7.6E-03	4.6E-02	-	-	-	-	1.7E-03	7.5E-05	-
IKHL2-9	Sphalerite	2.0E-02	3.2E-02	1.4E-01	7.1E+00	-	-	-	3.3E-03	1.1E-04	-
IKHL1-3	Sphalerite	1.5E-02	4.3E-02	1.7E-01	1.1E+01	-	-	-	5.2E-03	1.6E-04	-
IKHL1-3	Sphalerite	1.8E-02	2.4E-02	2.0E-01	1.1E+01	-	-	-	6.7E-03	2.9E-04	-
IKHL1-3	Sphalerite	9.1E-03	1.9E-02	8.0E-02	8.8E+00	-	-	-	3.1E-03	2.8E-05	-
IKHL1-3	Sphalerite	1.5E-02	4.7E-02	1.5E-01	1.0E+01	-	-	-	4.7E-03	1.7E-04	-
IKMV1-4	Sphalerite	1.9E-02	2.1E-02	1.6E-01	8.6E+00	-	-	-	6.0E-03	-	-
IKMV1-4	Sphalerite	1.1E-02	4.8E-03	-	-	-	-	-	6.2E-03	1.3E-04	-
IKMV1-4	Sphalerite	1.1E-02	3.7E-02	1.8E-01	1.6E+01	-	-	-	7.1E-03	2.4E-04	-
IKHL1-3-3B	Sphalerite	1.8E-03	3.1E-02	4.3E-02	2.4E+01	-	-	-	1.4E-03	2.6E-05	-
IKHL1-3-3C	Sphalerite	1.7E-02	3.7E-02	1.4E-01	8.5E+00	-	-	-	4.9E-03	1.3E-04	-
IKHL1-3-3D	Sphalerite	1.8E-02	3.8E-02	1.6E-01	8.8E+00	-	-	-	5.4E-03	1.1E-04	-
IKHL1-3-3E	Sphalerite	1.3E-02	2.9E-02	1.6E-01	1.2E+01	-	-	-	5.8E-03	-	3.6E-04
IKHL1-3-3F	Sphalerite	2.0E-02	3.5E-02	1.8E-01	9.0E+00	-	-	-	5.6E-03	1.1E-04	-
IKMV2-12-2A	Sphalerite	1.6E-02	1.5E-02	1.3E-01	8.2E+00	-	-	-	4.9E-03	8.0E-05	-
IKMV2-12-2B	Sphalerite	1.7E-02	1.7E-02	1.5E-01	8.5E+00	-	-	-	5.6E-03	5.6E-05	6.7E-05
IKMV2-12-2C	Sphalerite	1.7E-02	-	1.1E-01	6.6E+00	-	-	-	4.3E-03	5.6E-05	-
IKMV2-12-2D	Sphalerite	1.9E-02	2.2E-02	1.4E-01	7.1E+00	-	-	-	4.9E-03	6.7E-05	-

Table 4: List for atomic ratios calculated from the elemental concentrations LA-ICP-MS.

In order to look for relationships between fluid inclusion composition and the microthermometry data, the concentrations of the six most consistently detectable elements, Na, Ca, K, Mg, Ba, and Sr, were converted to atomic ratios with Na in the denominator, and were plotted versus homogenization temperature and salinity (Figure 7). All of the data plotted in Figure 7 are from episodes II and III, as analyses of the episode IV calcite-hosted fluid inclusions did not yield quantifiable results. All five atomic elemental ratios plot as elongated arrays over a homogenization temperature range of about 100 to 165 °C and a salinity range of about 14 to 24 eq. wt% NaCl that suggests mixing principally between two saline end member fluids (F1 and F2), but with enough of a contribution from a third, probably more dilute fluid (F3) to cause the data to deviate from one-dimensional arrays to more scattered two-dimensional arrays. The composition of these end member fluids cannot be determined with much precision given the scatter of the data. However, by considering where the data fields intersect a salinity of about 23 eq. wt% NaCl and a homogenization temperature of about 150 °C, the compositions of the F1 and F2 fluids can be estimated. These intersection intervals for the atomic ratios, Ca/Na, K/Na, Mg/Na, and Sr/Na, are similar within the resolution of data, indicating that the major element compositions of the F1 and F2 fluid were probably similar to one another.

Figure 8 compares the compositions of fluid inclusions from the Illinois-Kentucky district to those of fluid inclusions from MVT deposits in the Ozark Plateau. Though the Illinois-Kentucky fluid inclusion compositions overlap those of the Ozark MVT districts, the Illinois-Kentucky fluid inclusion compositions overall are clearly distinct, with higher atomic ratios of Ba/Na, Ca/Mg, Ca/Na, K/Na, Sr/Na, and lower atomic ratios of Mg/Na. This distinct fluid chemistry may correspond to the distinct mineral assemblage of the Illinois-Kentucky district relative to the Ozark MVT districts. In addition, sphalerite- and fluorite-hosted fluid inclusions in the Illinois-Kentucky district differ significantly from one another, with the sphalerite-hosted

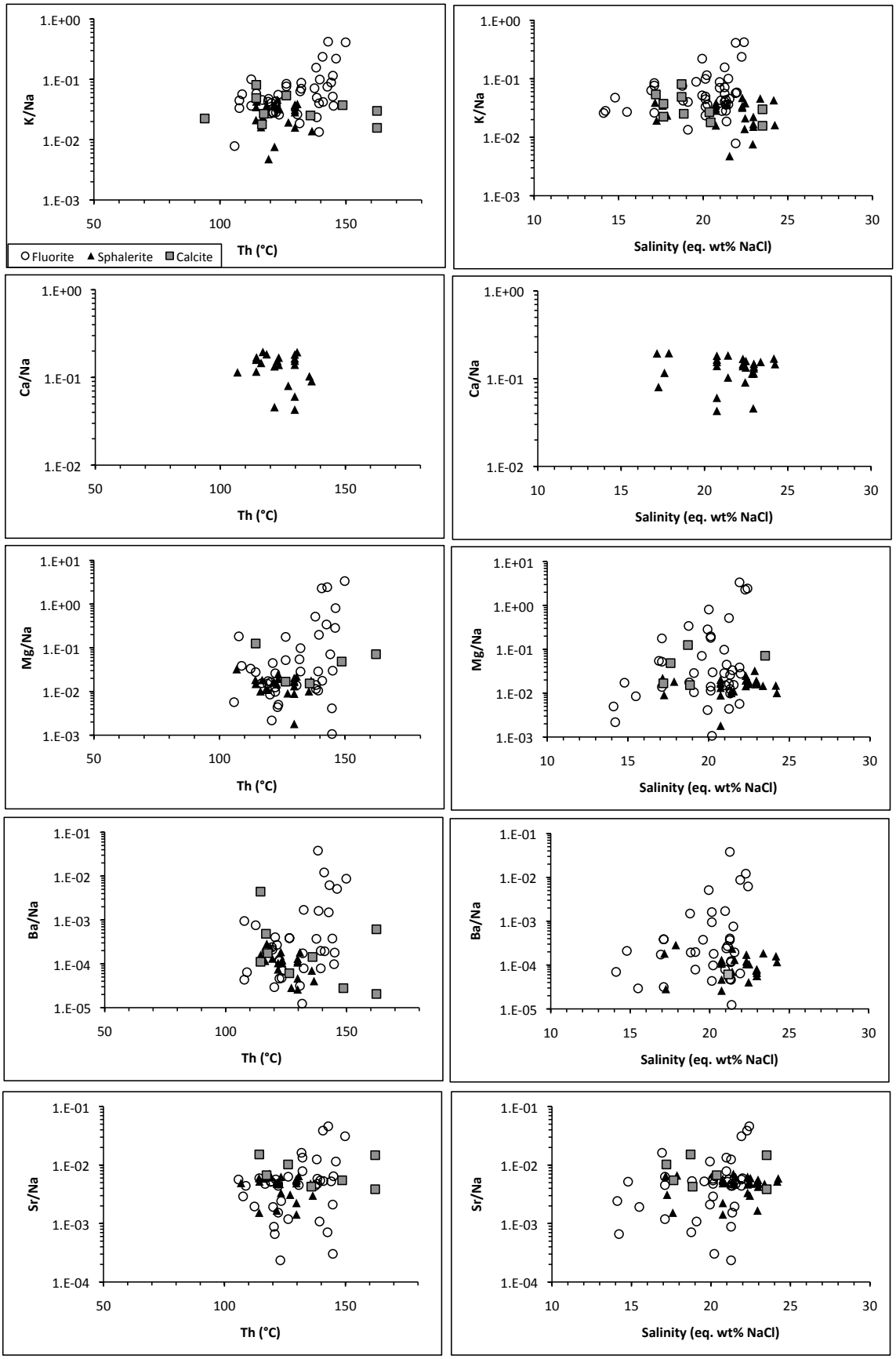

Figure 7: Elemental concentrations plotted as a function of homogenization temperature and salinity. The same symbol legend applies to all of the plots.

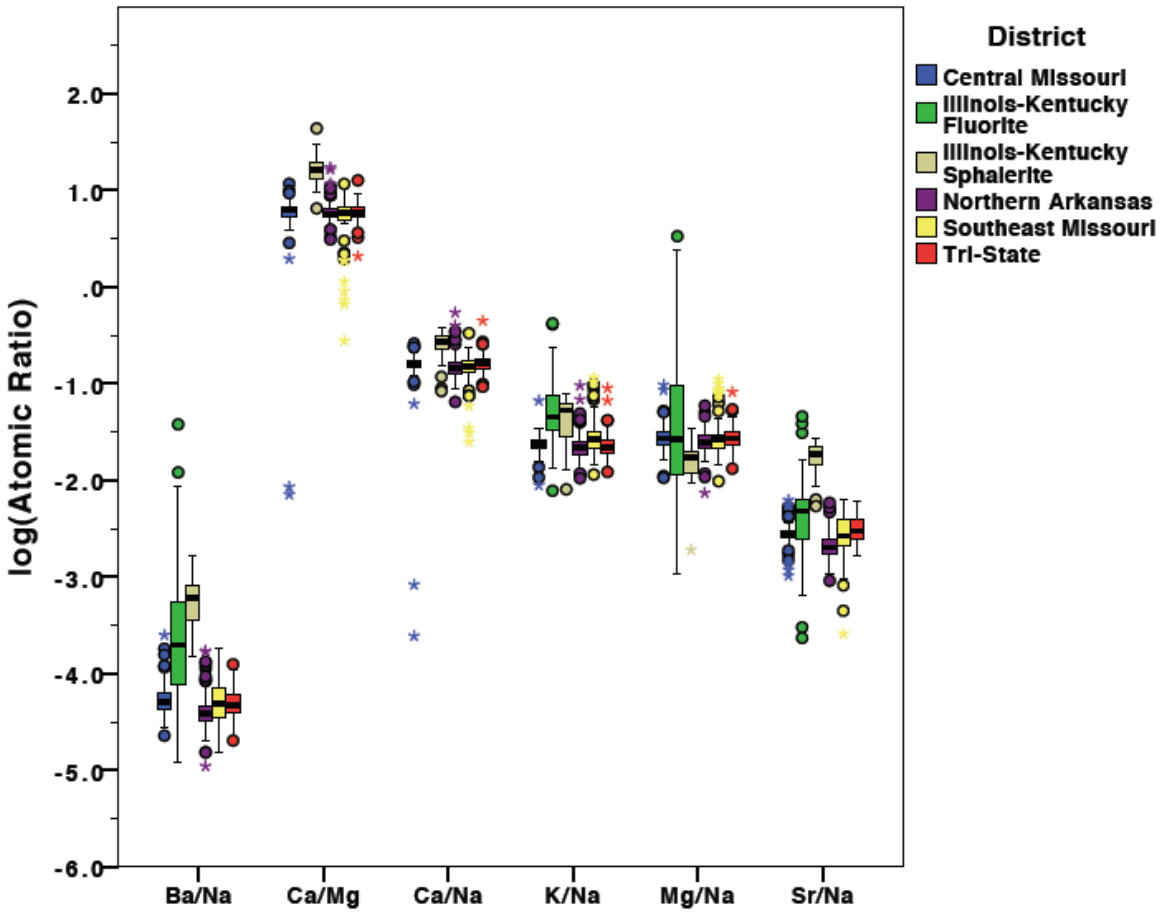

Figure 8: Box plot of the atomic ratio of Ca/Mg and the atomic ratios of Ba, Ca, K, Mg, and Sr to Na for fluorite- and sphalerite-hosted fluid inclusions from the Illinois-Kentucky district determined from the present study, and from sphalerite-hosted fluid inclusions from the Ozark MVT districts determined by Wenz (2011). Ca/Na and Ca/Mg ratios for fluorite-hosted fluid inclusions are not reported because of the interference of Ca from the host matrix.

fluid inclusions tending to have higher Ba/Na and Sr/Na ratios.

The Ba/Na ratios of fluid inclusions from the Illinois-Kentucky district on the whole are significantly higher than those of fluid inclusion from the Ozark MVT districts. This is consistent with the much larger proportion of barite mineralization found in the Illinois-Kentucky district compared to Southeast Missouri, Tri-State, and Northern Arkansas districts. The Central Missouri district of the Ozark Plateau is predominantly a barite district, so the reason for its lower Ba/Na ratios is less clear. Barite production records for the Illinois-Kentucky district are not available, but it is possible that the higher Ba/Na ratios in Illinois-Kentucky district may correlate to a greater mass of barite mineralization compared to the Central Missouri district where total barite production has amounted to only 350,000 tons (Viets and Leach, 1990).

Sphalerite-hosted fluid inclusions from the Illinois-Kentucky district are relatively more calcium-rich than sphalerite-hosted fluid inclusions from the Ozark MVT districts. The Ca/Mg ratio for Illinois-Kentucky fluid inclusions ranges from 3.5 to 23.7 with a median of 16.6 whereas for the Ozark MVT districts ranges about 0.01 to 17.3 (Wenz, 2011). The Ca/Mg ratios from the Illinois-Kentucky district are less than 34 which is the maximum value at which dolomite would replace calcite (Appold and Wenz, 2011). Thus, the fluid responsible for precipitating sphalerite in the Illinois-Kentucky district was dolomitizing, but not as dolomitizing as the fluids that precipitated sphalerite in the Ozark Plateau. This is consistent with the generally much greater abundance of dolomite in the Ozark MVT districts compared to the Illinois-Kentucky district. Nonetheless, the dolomitizing character of the sphalerite-hosted fluid inclusions from the Illinois-Kentucky district indicates that the fluid that precipitated sphalerite could not have traveled very far in the present Mississippian limestone ore host rocks, or the fluid would have equilibrated with calcite. Instead, the fluid must have traveled to the district through non-limestone aquifers, and based on the geologic evidence cited earlier, ascended via faults and fractures into the limestone ore host rocks.

The fluorite- and sphalerite-hosted fluid inclusions from the Illinois-Kentucky district have similarly elevated K/Na ratios compared to fluid inclusions from the Ozark MVT deposits, which are already elevated compared to typical sedimentary brines (Sverjensky, 1986). Elevated K concentrations in MVT ore fluids have been interpreted to indicate that fluids originated from deeper and hotter parts of sedimentary basins (Hanor, 1979; Appold Wenz, 2011). In the Illinois-Kentucky district, an additional factor may be the abundance of alkaline lamprophyre and peridotite intrusions, which Bradbury (1962) has determined to have K_2O contents ranging from 0.4 to 2.4 weight percent. As the parent magmas of these rocks cooled, they may have released K-rich fluids into ore forming sedimentary brines, elevating their overall K content. Alternatively, if mineralization was later rather than contemporaneous with igneous activity, the sedimentary brines may have acquired elevated K contents through partial alteration of the igneous intrusions.

The abundance of ultramafic igneous rocks in the Illinois-Kentucky district does not in general seem to have led to elevated Mg concentrations in the ore fluids. The Mg/Na ratios of Illinois-Kentucky fluid inclusions on average are similar to or slightly lower than those of Ozark MVT fluid inclusions, though the Mg/Na ratios of fluorite-hosted fluid inclusions from the Illinois-Kentucky district vary much more widely than those of other fluid inclusions. If mineralization was contemporaneous with igneous activity in the Illinois-Kentucky district the reason that Mg concentrations are not higher in the fluid inclusions may be that Mg is a much more compatible element than K so that less Mg would have been expelled from the magmas as it cooled. Elements like K, Rb, Sr, Ba, and rare earth elements are not compatible within major rock forming minerals and become concentrated in magma residuals, whereas elements such as Mg and Fe are highly compatible and become concentrated in mineral constituents as the magma crystallizes (Faure, 1998). Alternatively, if mineralization post-dated igneous activity, the reason Mg concentrations in the fluid inclusions are not higher may be a function of the alteration process. Most of the igneous intrusions in the district have been serpentinized (Bradbury, 1962),

a process that does not necessarily release Mg into solution (Best, 1982). If the MVT brines were responsible for this serpentinization it may explain why they did not become more Mg-rich. Alternatively, if the igneous intrusion had already been altered before they came into contact with the MVT brine, the rocks may have been resistant to further alteration that could have released Mg into solution.

Both the fluorite- and sphalerite-hosted fluid inclusions from the Illinois-Kentucky district have elevated Sr concentrations relative to fluid inclusions from the Ozark MVT districts. This difference may be explained by the abundance of lamprophyre and mica peridotite intrusions in the Illinois-Kentucky district. Lamprophyres in general tend to be enriched in Sr (Andrinov and Foley, 2000; Winter, 2001), and Bradbury (1962) found the igneous intrusions in the Illinois-Kentucky district to contain Sr in concentrations ranging from 500 to 2000 ppm. These concentrations are significantly greater than the concentration of Sr in ultramafic rocks (5.5 ppm) or even of mafic (450 ppm), granitic (440 ppm), or carbonate rocks (610 ppm; Faure, 1998), suggesting that concentrations are significantly greater than the average concentration of Sr in igneous rocks and that the igneous intrusions in the Illinois-Kentucky district could have been a significant potential source of Sr either during their crystallization or alteration.

Paragenetic Variations in Concentrations of Aqueous K, Mg, Sr, and Ba

Figure 9 shows box plots of the atomic ratios, K/Na, Mg/Na, Sr/Na, and Ba/Na, in fluid inclusions as a function of paragenetic stage. The atomic ratios show large, order of magnitude-scale variation at most paragenetic stages, indicating that mixing among fluids with very different concentrations must have been occurring throughout the paragenesis. Within this high variability some broad patterns are nonetheless evident. Fluid inclusions hosted by episode II fluorite tend to have lower K/Na, Mg/Na, and Ba/Na ratios than fluid inclusions hosted by episode III fluorite. Sphalerite- and calcite-hosted fluid inclusions have lower K/Na, Ba/Na, and higher Sr/Na ratios than most of the fluorite-hosted fluid inclusions. The elemental concentration data in Figure 9 do

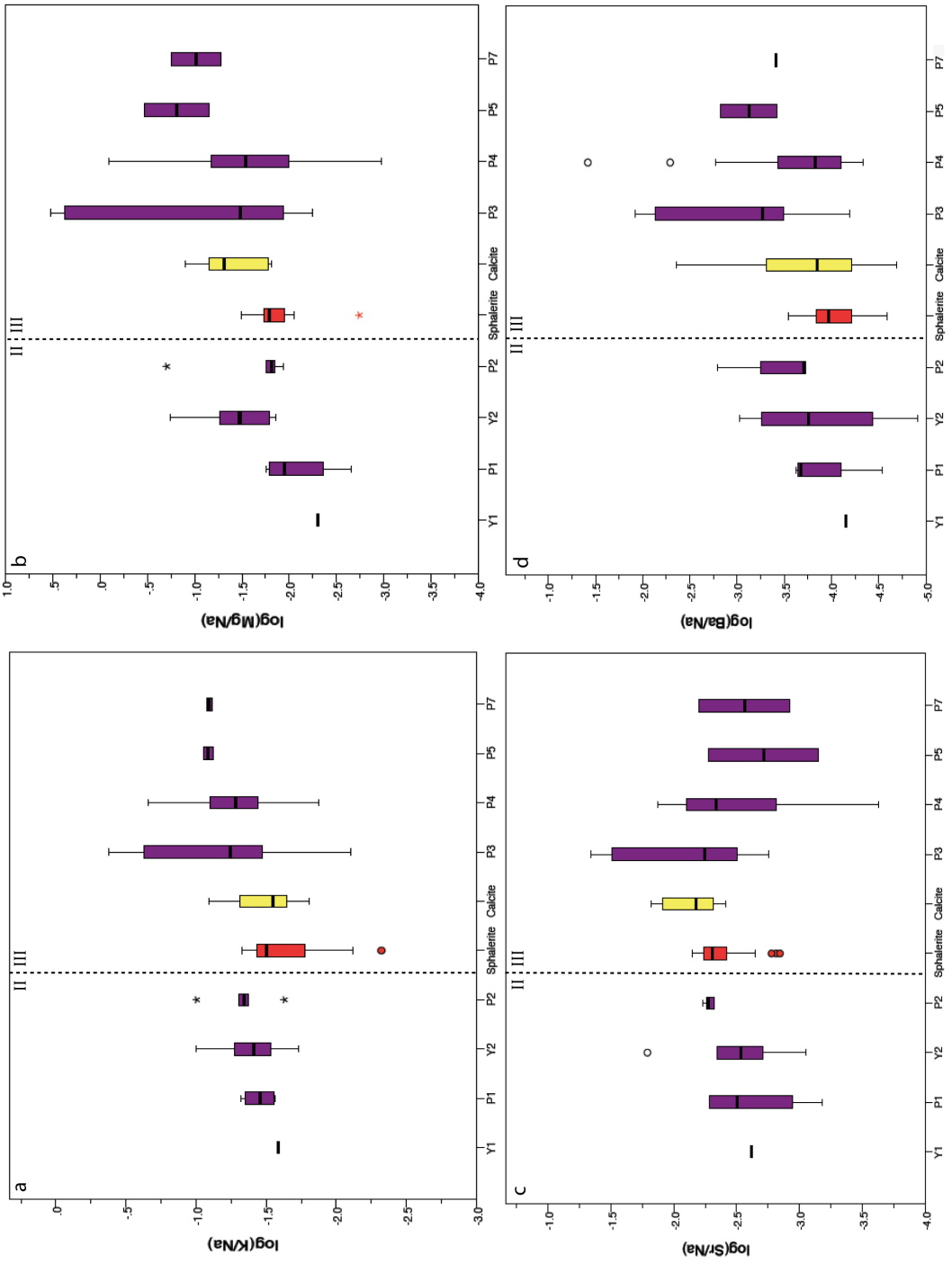

Figure 9: Box plots showing atomic ratios of (a) K/Na, (b) Mg/Na, (c) Sr/Na, and (d) Ba/Na in fluid inclusions as a function of the paragenetic stage of the host mineral.

not correlate strongly to salinity as a function of paragenesis data shown in Figure 5, though this may partly be a function of the number of analyses. The data in Figure 5 suggest that a dilute contribution is most strongly evident during the earliest stage of fluorite deposition (Y1 and P1) as well as the latest (P6 and P7). In Figure 9, Y1 and P1 fluorite-hosted fluid inclusions may be distinguishable relative to Y2 and P2 through P5 fluorite deposition. However, no P6 and only four P7 fluorite-hosted fluid inclusions were analyzed so that any trend during this stage of paragenesis would be difficult to discern.

Paragenetic Variations in Aqueous Concentrations of Pb, Zn, Cu, and Fe

Unlike Ba, the aqueous concentrations of the ore metals, Pb, Zn, Cu, and Fe, were not consistently measurable in the fluid inclusions analyzed. In sphalerite-hosted fluid inclusions, Zn, Cu, and Fe concentrations were never quantifiable due to matrix interference. However, Pb concentration was quantifiable in some fluid inclusions, reaching a maximum value of 184 ppm. In fluorite-hosted fluid inclusions, absolute ore metal concentrations could be estimated from the atomic ratios by assuming a Na concentration of 64,000 ppm, the average of the sphalerite-hosted fluid inclusions. This resulted in maximum ore metal concentrations of Pb = 1800 ppm, Zn = 2600 ppm, Cu = 1900 ppm, and Fe = 5000 ppm.

An important consideration concerning the calculated metal concentrations is whether they truly represent aqueous concentrations or reflect contamination from solid solution or mineral inclusions in the host mineral matrix. A preliminary assessment of this question was made by examining samples of fluorite and sphalerite with a Hitachi S4700 field emission scanning electron microscope at the University of Missouri−Columbia. The examination revealed some sections of fluorite crystals to have high densities of sub-micrometer sulfide and barite mineral inclusions (note bright spots in the back-scattered electron image Figure 10), whereas other sections had no detectable mineral inclusions. Mineral inclusions in the sphalerite

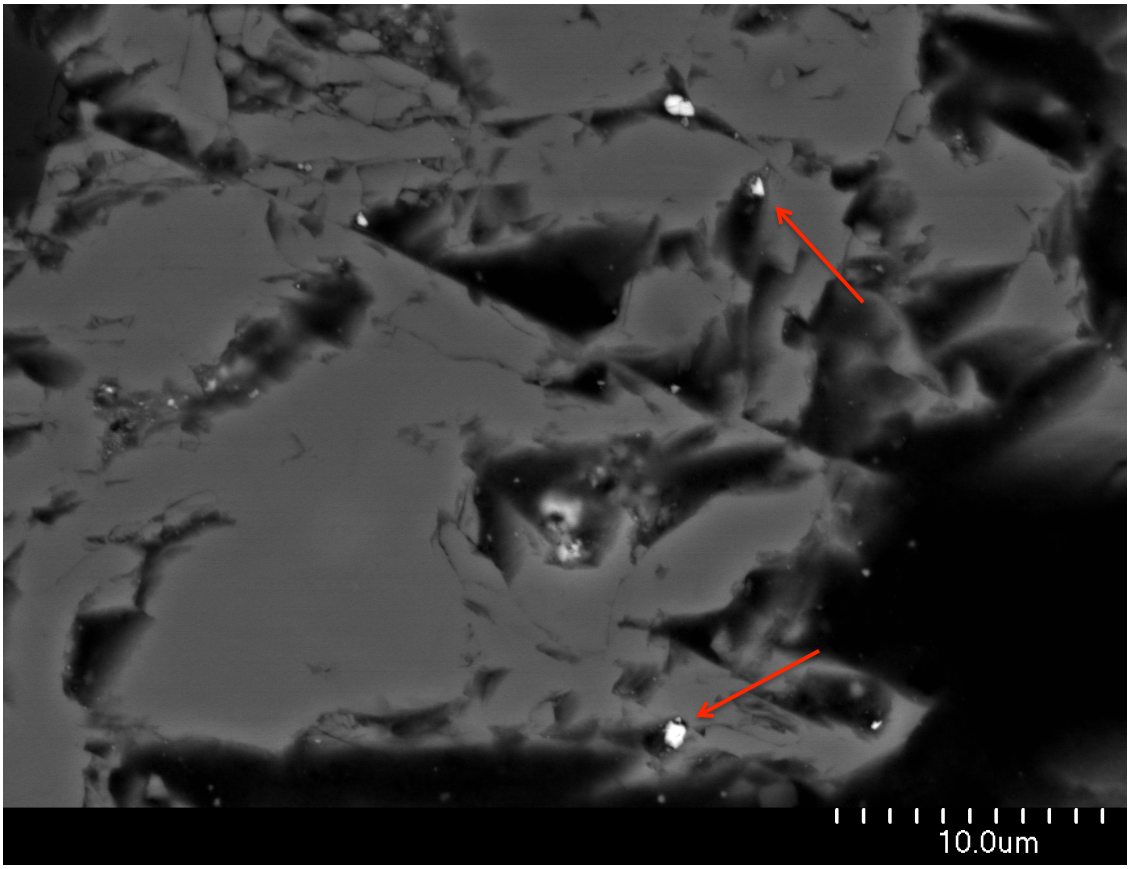

Figure 10: Back scattered electron image of fluorite from the Minerva mine. Length scale is shown in the lower right corner of the image. Bright micrometer- to submicrometer-scale spots, highlighted by red arrows, represent barite and sulfide mineral inclusions.

samples analyzed were rare. These finding indicate that metal concentrations obtained from bulk crush leachate analysis of fluorite-hosted fluid inclusions in previous studies (Czamanske et al., 1963; Pinckney and Haffty, 1970) have a high probability of having been contaminated by mineral inclusions in the host mineral matrix.

To try to determine whether ore metal signals from the LA-ICP-MS analyses were aqueous in origin or products of mineral inclusions or solid solution in the host mineral matrix, time series plots of signal intensity like the spectra shown in Figure 11 were examined. Ore metal signals are most likely to have originated from fluid inclusions when they correlate strongly to the signals of known aqueous constituents like Na, instead of matrix constituents like Ca in the case of fluorite and calcite and Zn in the case of sphalerite. For each analysis shown as well as for others not shown but reported in Table 3, the positions and shapes of the ore metal signal responses correlate strongly with that of Na, indicating that the ore metal signals are probably aqueous. Thus, at least one of the fluids involved in MVT in the Illinois-Kentucky district is likely to have been metal-rich, and at least one of the fluids is likely to have been metal-poor.

Figure 12 shows a box plot of atomic ratios of Cu, Fe, Pb, and Zn relative to Na in fluid inclusions as a function of paragenetic stage of the host mineral. Though the ratios are highly variable and though fluid inclusions with metal concentrations below the instrumental detection limits are not accounted for in the plot, a general trend of higher metal concentrations in the later portions of the paragenesis is discernable, i.e. fluid inclusions with high metal concentrations are more common in the later parts of the paragenesis. These higher metal concentrations post-date most of the period of main stage sulfide deposition, which coincides with Y2 to the beginning of P3 fluorite deposition (Figure 2). Thus, higher ore metal concentrations in fluid inclusions do not correlate with the period of their respective sulfides at Cave-in-Rock, but they do roughly correlate with higher K/Na, Mg/Na, and Ba/Na ratios.

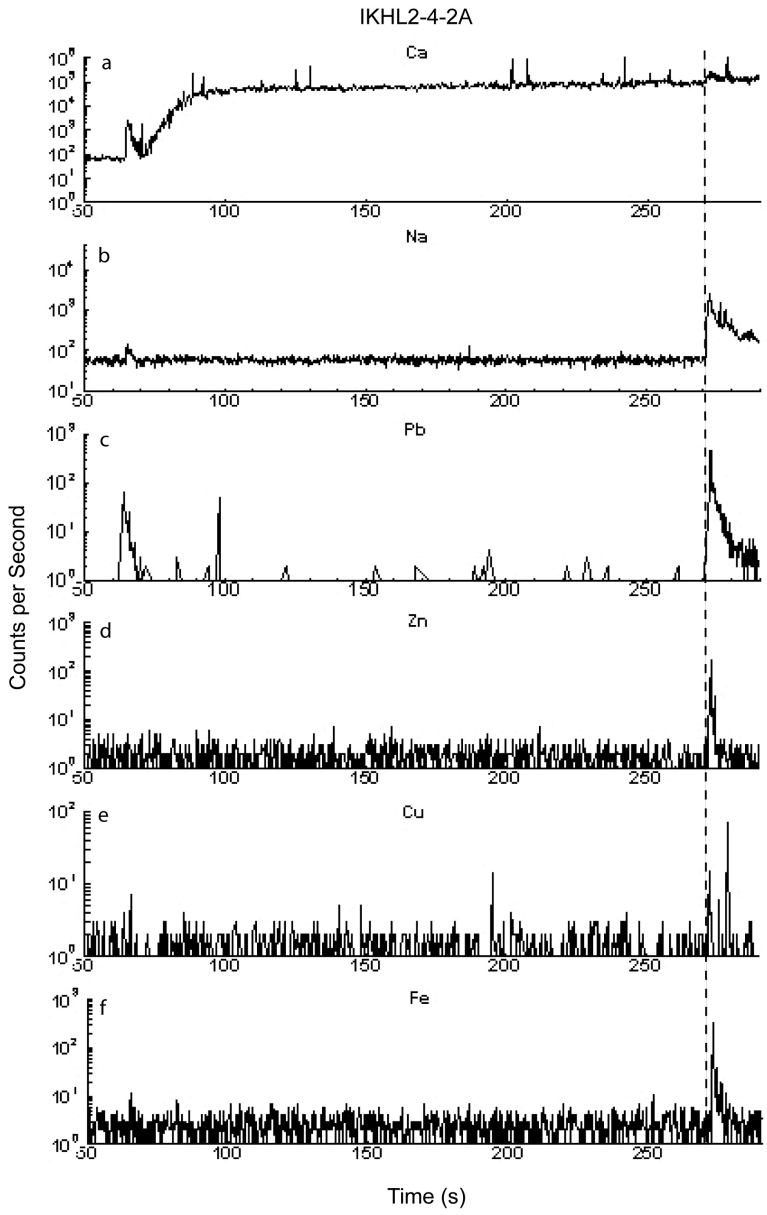

Figure 11: Transient signal response of (a) Ca, (b) Na, (c) Pb, (d) Zn, (e) Cu, and (f) Fe from LA-ICP-MS analyses of a fluorite-hosted fluid inclusion, IKHL2-4-2A. The vertical dashed line through the plots denotes the beginning of ablation of the target inclusion. The signals of Pb, Zn, and Fe correlate well with the signal of Na, indicating an aqueous origin for these three metals. The Ca signal also rises slightly at the Na peak, indicating the presence of some Ca in solution in the fluid inclusion. The Cu signal is more ambiguous as it does not match the shape of the Na well.

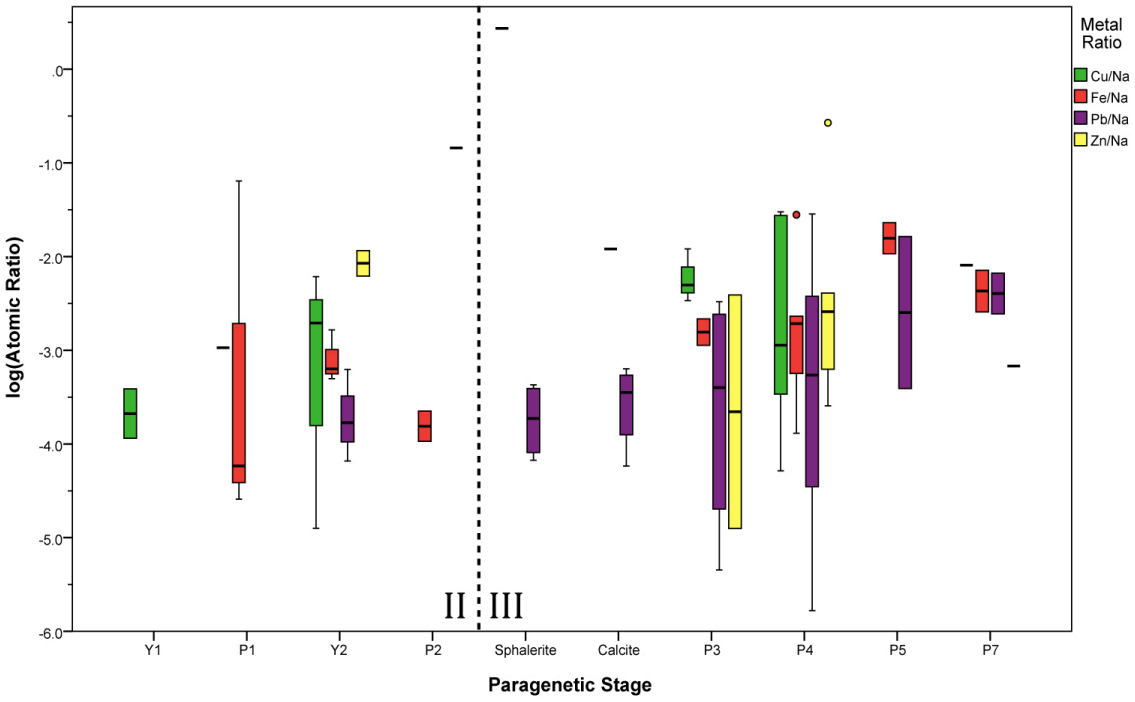

Figure 12: Box plot of detectable atomic Cu/Na, Fe/Na, Pb/Na, and Zn/Na ratios in fluid inclusions as a function of paragenetic stage of the host mineral.

Raman Microprobe Analysis

Raman spectroscopy was performed on a total of 54 Type I fluid inclusions hosted by calcite, P1 through P7 fluorite, and sphalerite in order to estimate their methane concentrations, which could be used to estimate the depths of mineralization. Of the 54 fluid inclusions analyzed, 42 yielded quantifiable results. Raman analysis was performed at the Virginia Polytechnic Institute and State University in Blacksburg, VA using a JY Horiba LabRam HR (800 mm) spectrometer, with 1800 grooves/mm gratings and a slit width of 150 μm, resulting in a spectral resolution of ±1.37 cm^{-1} (Paroli and Butler, 1990). Excitation of the fluid inclusions was carried out using a 514.53 nm Laser Physics 100S-514 Ar^{+} laser. The laser was focused through a 3.5x objective with a working distance of approximately 12mm. The laser output was 50 mW at the source and less than 10 mW at the sample. The detector was an electronically cooled open electrode charge coupled device (CCD). A neon light source was channeled directly into the objective and its resultant peak positions were used to calculate the true methane peak positions. Due to the nonlinear behavior of the monochromator the laser was calibrated to the spectral region of interest in order to maximize the accuracy of the measured methane peaks. Three accumulations of 15 seconds were used to measure methane and neon peak positions. The position of the Raman line was determined after baseline correction using parameters for Guassian/Lorentzian peak fitting described in Lin et al. (2007). The positions of the two neon peaks and methane peak, along with ambient room temperature, homogenization temperature, and salinity of the fluid inclusions were used to calculate the saturated concentration and trapping pressure of methane following the procedure of Becker et al. (2010).

Results

The results of the Raman microprobe analysis are shown in Table 5, including the raw and adjusted, by the method described by Becker et al. (2010), methane wave number peak location, the total aqueous methane concentration, the saturation pressure for this methane concentration, which is assumed to be the trapping pressure of the fluid inclusion, and the

Sample ID	Paragenetic Phase	Neon 1 (cm^{-1})	Neon 2 (cm^{-1})	Methane (cm^{-1})	Corrected CH4 (cm^{-1})	[CH_4] (ppm)	P_{EH} (bars)	Depth (m)
IKHL2-1-8A	Calcite	2849.91	2971.38	2916.59	-	-	-	-
IKHL2-1-2A	Calcite	2850.58	2971.43	2916.42	2917.33	574.81	94.51	964
IKHL2-1-3A	Calcite	2850.37	2971.41	2916.71	-	-	-	-
IKHL2-1-5D	Calcite	2850.33	2971.40	2916.60	-	-	-	-
IKHL1-12-2A	P1	2849.62	2970.61	2915.58	2917.38	543.98	74.11	756
IKHL1-12-6C	P1	2849.64	2970.63	2915.80	2917.58	484.30	63.46	648
IKHC1-12-3A	P1	2850.46	2971.39	2916.70	-	-	-	-
IKHC1-12-3B	P1	2850.49	2971.40	2916.50	2917.47	382.57	54.55	557
IKHC1-12-3C	P1	2850.46	2971.39	2916.57	2917.56	140.29	16.76	171
IKHC1-12-6F	P1	2850.57	2971.40	2916.68	-	-	-	-
IKHC1-12-6G	P1	2850.57	2971.41	2916.61	2917.53	153.74	24.61	251
IKHC1-12-6H	P1	2850.58	2971.41	2916.73	-	-	-	-
IKHL2-2-1B	P2	2849.61	2970.63	2915.70	2917.49	684.33	107.10	1093
IKHL2-21-3E	P2	2850.59	2971.41	2916.64	2917.55	136.67	20.17	206
IKHL2-21-3F	P2	2850.59	2971.42	2916,65	2917.56	123.03	18.37	187
IKHL2-21-3G	P2	2850.46	2971.41	2916.68	-	-	-	-
IKNG1-7-4C	P3	2850.55	2971.38	2916.62	2917.56	76.96	12.96	132
IKNG1-7-4A	P3	2850.56	2971.40	2916.79	-	-	-	-
IKNG1-7-4B	P3	2850.55	2971.39	2916.59	2917.53	156.82	25.16	257
IKHL2-6-1B	P4	2849.72	2970.69	2915.90	2917.61	473.74	69.16	706
IKHL2-7-2B	P4	2849.65	2970.68	2915.83	2917.57	431.75	69.78	712
IKHL2-7-4C	P4	2849.69	2970.64	2915.90	2917.65	408.34	57.47	586
IKNG1-7-1D	P4	2850.61	2971.46	2916.60	2917.47	230.19	40.78	416
IKNG1-7-1E	P4	2850.61	2971.52	2916.58	2917.43	329.33	59.58	608
IKNG1-7-2A	P4	2850.20	2971.40	2916.70	-	-	-	-
IKNG1-7-2B	P4	2850.58	2971.40	2916.69	-	-	-	-
IKNG1-7-2C	P4	2850.35	2971.38	2916.64	-	-	-	-
IKNG1-7-3A	P4	2850.57	2971.39	2916.58	2917.51	220.32	33.69	344
IKNG1-7-3B	P4	2850.54	2971.40	2916.54	2917.48	297.96	45.56	465
IKHL2-4-5A	P5	2850.15	2971.18	2916.18	2917.43	877.06	133.91	1366
IKHL2-4-5B	P5	2850.19	2971.19	2916.19	2917.41	916.17	140.17	1430
IKHL2-4-4A	P5	2850.59	2971.39	2916.53	2917.45	417.09	59.18	604
IKHL2-4-4B	P5	2850.27	2971.37	2916.24	2917.33	727.43	109.07	1113
IKHL2-4-4C	P5	2850.40	2971.38	2916.51	2917.53	193.55	27.56	281
IKHL2-4-5D	P5	2850.39	2971.38	2916.45	2917.47	348.69	48.53	495
IKHL2-4-3E	P5	2850.45	2971.38	2916.45	2917.44	427.77	60.14	614
IKHL2-4-3A	P6	2850.40	2971.38	2916.45	2917.47	354.66	48.47	495
IKHL2-4-3B	P6	2850.48	2971.38	2916.51	2917.49	310.84	41.30	421
IKHL2-4-3C	P6	2850.29	2971.36	2916.50	2917.59	41.18	7.12	73
IKHL2-4-6A	P6	2850.57	2971.39	2916.37	2917.30	908.80	121.19	1237
IKHL2-4-6B	P6	2850.56	2971.40	2916.48	2917.41	543.78	73.18	747
IKHL2-4-6C	P6	2850.51	2971.39	2916.60	2917.56	116.92	16.46	168
IKHL2-4-2A	P7	2850.62	2971.49	2916.52	2917.38	558.74	79.20	808
IKHL2-4-2B	P7	2850.59	2971.49	2916.51	2917.38	596.96	79.10	807
IKHL2-4-2C	P7	2850.60	2971.41	2916.88	-	-	-	-
IKHL2-4-2D	P7	2850.58	2971.40	2916.41	2917.33	692.04	97.24	992
IKHL2-4-2E	P7	2850.56	2971.40	2916.38	2917.31	739.48	105.18	1073
IKHL2-9-1A	Sphalerite	2849.60	2970.62	2915.73	2917.53	489.86	89.93	918
IKHL2-9-1B	Sphalerite	2849.60	2970.61	2915.75	2917.56	446.68	82.49	842
IKHL1-3-3A	Sphalerite	2849.52	2970.51	2915.29	2917.18	1171.83	245.52	2505
IKMV1-4-1A	Sphalerite	2849.55	2970.53	2915.47	2917.34	660.60	149.81	1529
IKMV1-4-4A	Sphalerite	2849.54	2970.56	2915.38	2917.24	1124.15	226.08	2307
IKMV1-4-4C	Sphalerite	2849.53	2970.59	2915.56	2917.41	671.21	128.46	1311

Table 5: Results of Raman microprobe analysis of methane in fluid inclusions and calculated trapping pressures and depths.

corresponding trapping depth of the fluid inclusions an thus the depth of mineralization, assuming hydrostatic conditions and a constant fluid density of 1000 kg/m^3.

A histogram of the calculated depths of mineralization is shown in Figure 13. The depths are mostly in the range of about 100 to 1500 m with two outlying values of 2300 and 2500 m that may be a result of entrapment of a separate, immiscible methane phase with liquid water saturated with respect to methane, so that the two fluid inclusions from which these outlying values were obtained may therefore not strictly be Type I fluid inclusions. The mean depth, not including these three outlying values is 680 m. A depth range of about 100 to 1500 m is large, but the higher values in this range are more likely to reflect the true depth of mineralization. This is because the methane pressure calculations assume that methane was saturated in the aqueous liquid at the time of fluid inclusion entrapment. If methane were actually undersaturated in the fluid, then any assumed pressure based on its aqueous concentration would be lower than the actual trapping pressure, and thus the corresponding trapping depth would also be too low. It is also possible that variable post-entrapment stretching of some of the fluid inclusions has reduced some of the calculated methane pressures. If the higher trapping depths of about 680 to 1500 m are more likely to be accurate than the lower trapping depths, then they are consistent with typical depths of MVT deposit formation of 600 to 1500 m (Sverjensky, 1986). Deposit formation depths in the range of 680 to 1500 m in the Illinois-Kentucky district are also consistent with Lower Permian age of mineralization suggested by the dating of Zartman et al. (1967), Snee and Hayes (1992), and Chesley et al. (1994), but depending on how much erosion has occurred since the end of the Permian the depths could also fit with a Jurassic-Cretaceous age suggested by Harder (1986), Ruiz (1988), and Symons (1994). These deposit formation depths however are not consistent with an age of mineralization coincident with the peak of Alleghanian sediment accumulation at the end of the Permian. This is illustrated by the results of Beaumont et al. (1987), who estimated through a combination of lithospheric flexural modeling, coal moisture

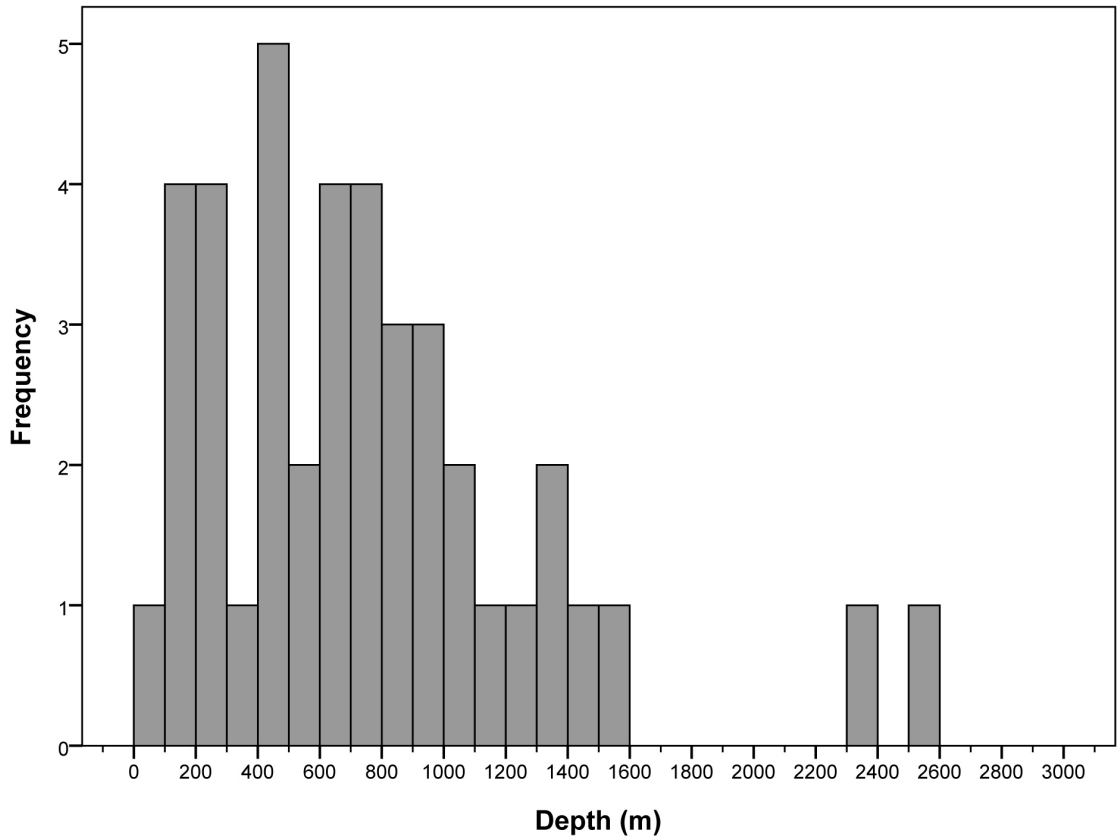

Figure 13: Histogram of the calculated depths of mineralization calculated from the partial pressure of methane within fluid inclusions determined by Raman microprobe analysis.

content analysis, and fission track thermochronometry that about 200 m of Chesterian (Upper Mississippian) sediments and about 900 m of Pennsylvanian sediments were originally deposited in the Illinois-Kentucky district, thus totaling about 1100 m of overburden above the district's MVT deposits, which are hosted by Velmeyeran and Lower Chesterian rocks. However, by the end of the Permian, about another 900 m of sediments had been deposited in the Illinois-Kentucky district, bringing the overburden thickness above the MVT deposits to about 2000 m, which exceeds the main range of calculated depths of mineralization. However, it is possible that at least 500 m of this overburden could have been eroded away by the Jurassic or Cretaceous, so that these later dates of mineralization are also possible based on the present estimates of the depth of mineralization.

Discussion

The results of the present study indicate that the fluids that formed the MVT deposits in the Illinois-Kentucky district are chemically distinct from the fluids that formed MVT deposits in the adjacent Ozark Plateau. Mineralizing fluids in the Illinois-Kentucky district tend to be slightly more dilute than mineralizing fluids in the Ozark MVT districts (Wenz, 2011) and tend to have higher K/Na, Ca/Na, Ca/Mg, Ba/Na, and Sr/Na ratios but lower Mg/Na ratios. These differences parallel the results of Kendrick et al. (2002), who found mineralizing fluids from the Illinois-Kentucky district to contain higher $^{40}Ar/^{36}Ar$ and I/Cl ratios than mineralizing fluids from the Viburnum Trend or Tri-State district, and therefore concluded the Illinois-Kentucky and Ozark MVT deposits to have formed from separate fluids. The differences in fluid composition may in part be attributable to the fluids having had different source basins and flow paths where they interacted with rocks of significantly different compositions. For example, numerous geochemical indicators cited by Leach (1994) and hydrologic modeling carried out by Bethke et al. (1988), Garven et al. (1993), Appold and Garven (1999), and Appold and Nunn (2005) point to the Arkoma basin and adjacent platform as having been the source of MVT mineralizing fluids

in the Ozark Plateau, whereas Pb isotope data from Goldhaber et al. (1995) link mineralizing fluids in the Illinois-Kentucky district to the Illinois basin.

A further contributing factor to the differences in fluid composition may be the presence of ultramafic igneous intrusions in the Illinois-Kentucky district, which are not found in the Ozark MVT districts. Support for the involvement of this deep-seated, rift-related magmatism in the MVT mineralization in the Illinois-Kentucky district comes from Kendrick et al. (2002), who measured $^{3}He/^{4}He$ ratios in fluorite-hosted fluid inclusions from the district and found them to be elevated above typical crustal values, consistent with a mantle-derived component of helium accounting for up to 6% of the total helium in the mineralizing fluid mixture. Further support for an igneous contribution to mineralization in the district comes from reaction path modeling by Plumlee et al. (1995), who showed that titration of magmatically derived HF-rich gases into sedimentary brine that subsequently cooled or mixed with a Ca-rich brine would produce a fluorite-rich, dolomite-poor mineral assemblage associated with extensive calcite dissolution characteristic of the Illinois-Kentucky district. Because lamprophyres, one of the principal igneous rock types in the district, crystallize from volatile-rich alkalic residual magmas that tend to be concentrated in K and trace elements like Sr and Ba (Bradbury, 1962; Winter, 2000), fluids exsolved from these magmas may have been correspondingly K-, Sr-, and Ba-rich, such that when the fluids became incorporated into sedimentary brines, the concentrations of these elements in the brines became elevated relative to Ozark MVT brines. Magmatic fluids could still have affected the composition of mineralizing fluids in the Illinois-Kentucky district, even if mineralization was Jurassic instead of Permian, the age of the exposed intrusions in the district. Plumlee et al. (1995) have suggested that if mineralization was Jurassic, then magmatic fluids could have been derived from deep, unexposed magmas generated during that time as a result of incipient rifting due to the breakup of Pangea.

The wide range of salinity and elemental compositions in fluid inclusions from the Illinois-Kentucky district strongly suggest that mineralization was produced from mixture of

chemically distinct fluids. Fuhrmann (1994) and Fuhrmann and Spry (1994) interpreted their micothermometry data to indicate mixing among three fluids, two of which were relatively saline and hot, and the third of which was significantly cooler and more dilute. The microthermometry data from the present study can be interpreted similarly, though the susceptibility of fluorite-hosted fluid inclusions to post-entrapment stretching likely would have weakened any compositional trends with homogenization temperature that may exist. Mixing among at least three fluids is also supported by the present study's LA-ICP-MS compositional data, which generally do not correlate strongly with one another, with salinity, or with homogenization temperature, but instead plot as broad two dimensional arrays in which the compositions of end member fluids are indistinct (Figure 7). The existence of any compositional variation as a function of paragenesis is unclear based on the relatively small number of analyses and large compositional variations at some of the paragenetic stages, though there may be broad if vague trends towards higher K, Mg, and ore metal contents in fluid inclusions trapped during episode III compared to episode II. Hall and Friedman (1963) investigated major element compositional variations in bulk crush leachates of fluid inclusions as a function of paragenesis. Their Ca/Na SO_4/Na trends were probably distorted by mineral matrix interferences from Ca in fluorite and oxidation of sulfide present in sphalerite and galena, respectively. The remainder of their compositional data is less likely to have been affected by mineral matrix contamination, though some degree of contamination from secondary fluid inclusions cannot be ruled out. Their atomic K/Na and Mg/Na ratios are similar in magnitude to the median atomic K/Na and Mg/Na ratios from the present study, though much less variable, but increase sharply during the precipitation of late (episode IV) barite and witherite, which were not analyzed in the present study. Hall and Friedman (1963) found D/H values to be lower in fluid inclusions from mineralization in episode III compared to episode II, which they interpreted to be a product of greater meteoric water input during episode III mineralization. Thus, it is possible that a fluid relatively enriched K, Mg, and

ore metals but more diluted by meteoric water contributed more strongly to mineralization during episode III than episode II.

Many of the LA-ICP-MS analyses returned ore metal signals above background, though many of those signals were not quantifiable into aqueous concentrations due to poor or ambiguous correlations with Na. Nonetheless, enough ore metal signals were quantifiable to indicate the presence of a population of metal-rich fluid inclusions, which suggests that at least one of the fluids involved in mixing in the Illinois-Kentucky district was metal-rich with concentrations as high as on the order of 1000s of ppm. Given that many of the fluid inclusions had undetectable concentrations of ore metals, at least one of the fluids involved in mixing must also have been metal-poor.

The presence of one or more fluids in the Illinois-Kentucky district that were at least metal-rich as some of the mineralizing fluids in the Ozark Plateau raises the question of why sulfide mineralization is not more abundant in the Illinois-Kentucky district. Based on the reaction path modeling of Plumlee et al. (1995), one reason may be that compared to the Ozark Plateau, the mineralizing fluid in the Illinois-Kentucky district was more acidic with a pH in the range of about 2 to 4, in which the solubilities of the ore metals, Pb, Zn, and Cu, would have been higher, inhibiting their precipitation. If sulfur concentration in the Illinois-Kentucky mineralizing fluid mixture was as high as the 1000's of ppm sulfate reported by Hall and Friedman (1963) for fluorite-hosted fluid inclusions, and assuming that this sulfate was originally sulfide that became oxidized during their experimental crushing and leaching process, then the pH must have been low in order for such high metal and sulfur concentrations to coexist. For example, calculations performed with Geochemist's Workbench^{TM} software (Bethke, 2004) show that for a 3 molal NaCl solution at 120 °C containing 3×10^{-2} m H_2S and 184 ppm Pb, the maximum calculated value for the sphalerite-hosted fluid inclusions, a pH of 1.8 would be needed to prevent galena from precipitating. Ore metals could remain in solution at much higher pH values if sulfur was present in the same concentrations as sulfate instead of sulfide. However, the abundance of

hydrocarbons in the Illinois-Kentucky district indicates reducing conditions to be have been more likely.

The fluorite dominated mineralogy of the Illinois-Kentucky district allowed the present study to obtain measurements of Zn, Cu, and Fe in fluid inclusions. The concentrations of these three metals have been difficult to constrain in fluid inclusions from other MVT deposits in the midcontinent because these three elements are abundant in the matrices of all of the ore-stage minerals in these other deposits. Results of the present study suggest that one or more metal-rich fluids in the Illinois-Kentucky district may have had Zn, Cu, and Fe concentrations as high as 2600 ppm, 1900 ppm, and 5000 ppm, respectively. The results of the present study also clearly showed that the Illinois-Kentucky mineralizing fluids differed from the Ozark MVT fluids with respect to their major element compositions so that differences in Zn, Cu, and Fe concentration are also possible. Nonetheless, the data give a first indication of the concentrations of these metals that were reached in midcontinent MVT ore forming systems.

Raman microprobe analysis has indicated that the trapping depths for mineral deposits from the Illinois-Kentucky district are in agreement with trapping depths calculated for other MVT ore deposits. The calculated trapping depths are in line with sediment thickness that supports an age of mineralization that is contemporaneous with igneous activity. If the trapping depth, and the earlier age of mineralization are accurate, then sedimentation would have continued on after the formation of bedded replacement deposits. This may provide an explanation to the broad range of homogenization temperatures obtained from fluid inclusions because the continued deposition of sediments would have caused the fluid inclusions to be heated above beyond their trapping temperatures.

Conclusions

The present study has shown that the Illinois-Kentucky district is a chemically distinct MVT deposit that is the result of sedimentary brine interacting with ultramafic rift-related igneous material that is K-, Sr-, and Ba-rich. The Illinois-Kentucky district has higher Ba/Na,

Ca/Mg, Ca/Na, K/Na, and Sr/Na and lower Mg/Na than districts in the Ozark Plateau. The higher Ca/Na and Ca/Mg atomic ratios from the Illinois-Kentucky district show that the mineralizing fluids from Illinois-Kentucky were less dolomitizing than the mineralizing fluids from the adjacent Ozark Plateau.

Though the current study was unable to determine any definitive paragenetic trends in elemental concentrations, broad elemental patterns were apparent. The data show that mineralizing fluids from the earliest episode of deposition, episode II, tended to have lower K/Na, Mg/Na, and Ba/Na ratios than fluids during episode III deposition. Fluids that precipitated sphalerite and calcite stages tended to have lower K/Na, Ba/Na, and Sr/Na ratios than fluids that deposited fluorite. No covariance between any of the most reliably detectable elements was discernable. Concentrations of ore metals in the fluid inclusions vary over orders of magnitude from 10s to 1000s of ppm, and possibly increasing from episode II to episode III.

Ore precipitation in the Illinois-Kentucky district probably involved mixing of at least three chemically distinct fluids, based on three populations of fluid inclusions evident from the microthermometry data and the broad two-dimensional arrays present in the compositional plots. Though metal sulfide and barite inclusions are common in much of the fluorite, high aqueous ore metal concentrations were identified in some fluid inclusions indicating that at least one fluid involved in mixing was likely metal-rich.

Results from Raman microprobe analysis suggest that the MVT mineralization in the Illinois-Kentucky district formed between 100 and 1500 m, but more likely between the mean depth of 680 m and 1500 m. These values are consistent with formation depths determined for other MVT deposits and with regional stratigraphic reconstructions. The high concentrations of methane and Fe in the fluid inclusions also suggest that the mineralizing fluids in the Illinois-Kentucky district were most likely reducing.

References

Andronikov, A. V., and Foley, S. F., 2000, Trace element and Nd-Sr isotopic composition of ultramafic lamprophyres form the east Antarctic Beaver Lake area: Chemical Geology, v. 175, p. 291-305.

Appold, M. S., Garven, G., 1999, The hydrology of ore formation in the southeast Missouri district: Numerical models of topography-driven fluid flow during the Ouachita orogeny: ECON. GEOL., v. 94, p. 913-935.

Appold, M S., and Nunn, J. A., 2005, Hydrology of the western Arkoma basin and Ozark platform during the Ouachita orogeny: Implications for Mississippi Valley-type ore formation in the Tri-State Zn-Pb district: Geofluids, v. 5, p. 308-325.

Appold, M. S., and Wenz, Z. J., 2011, Composition of ore fluid inclusions from the Viburnum Trend, Southeast Missouri district, United States: Implications for transport and precipitation mechanisms: ECON. GEOL., v. 106, p. 55-78.

Bastin, E. S., 1931, The fluorspar deposits of Hardin and Pope counties, Illinois: Illinois Geologic Survey Bull. v. 58, p. 116.

Beaumont, C., Quinlin, G. M., and Hamilton, J., 1987, The Alleghanian orogeny an its relationship to the evolution of the eastern interior, North America: *in* Beaumont, C. and Tankard, A. J. (Eds), Sedimentary Basins and Basin-Forming Mechanisms, Canadian Society of Petroleum Geologists, Memior 12, p. 425-445.

Becker, S. P., Eichhubl, P., Laubach, S. E., Reed, R. M., Lander, R. H., and Bodnar, R. J., 2010, A 48 m. y. history of fracture opening, temperature, and fluid pressure; Cretaceous Travis Peak formation, East Texas basin: Geological Society of America Bulletin, 122, 7-8, p. 1081-1093.

Best, M. G., 1982, Igneous and Metamorphic Petrology: W. H. Freeman, San Francisco.

Bethke, C. M., Harrison, W. J., Upson, C., and Altaner, S. P., 1988, Supercomputer analysis of sedimentary basins: Science, v. 239, p. 261-267.

Bodnar, R. J., 1993, Revised equation and table for determining the freezing point depression of H_2O-NaCl solutions: Geochimica et Cosmochimica Acta, v. 57, p. 683-684.

Bradbury, J. C., 1962, Trace elements, rare earths, and chemical composition of southern Illinois igneous rocks: Illinois State Geological Survey, circular 330.

Bradbury, J. C., and Baxter, J. W., 1992, Intrusive breccias at Hicks Dome, Hardin county, Illinois: Illinois State Geological Survey, circular 550.

Brown, J. C., Emery, J. A., and Meyer, P. A., Jr., 1954, Explosion pipe in test well on Hicks Dome, Hardin County, Illinois, ECON. GEOL., v. 49, p. 891-901.

Chelsey, J. T., Halliday, A. N., and Kyser, T. K., 1994, Rare earth element variations in fluorite: Investigation of the potential use of fluorite as a geochronometer [abs]: Terra Nova, v. 5, p. 454.

Cunningham, C. G., and Heyl, A. V., 1980, Fluid-inclusion homogenization temperatures throughout the sequence of mineral deposits in the Cave-in-Rock area, southern Illinois: ECON. GEOL. v. 75, p. 1226-1231.

Czamanske, G. K., Roedder, E., and Burns, F. C., 1963, Neutron activation analysis of fluid inclusions for copper, manganese, and zinc: Science, v. 140, p. 401-403.

Faure, G., 1998, Principles and Applications of Geochemistry, Second Edition: Prentice Hall Inc., 600 p.

Fuhrmann, G. D., 1994, Regional fluid inclusion study of the Illinois-Kentucky fluorspar district: Unpublished Masters thesis, Iowa State University, p. 79.

Garven, G., Ge, S., Person, M. A., and Sverjensky, D. A., 1993, Genesis of stratabound ore deposits in the mid-continent basins of North America. 1. The role of regional groundwater flow: American Journal of Science, v. 293, p. 497-568.

Goldstein, A., 1997, The Illinois-Kentucky fluorite district: The Mineralogical Record, v. 28, Jan.-Feb.

Goldstein, R. H., and Reynolds, T. J., 1994, Systematics of fluid inclusions in diagenetic minerals: Society of Economic Geologists and Paleontologists Short Course 31, 199 p.

Grogan, R. M., and Bradbury, J. C., 1967, Stratiform fluorite deposits of southern Illinois: ECON. GEOL. MON. 3, p. 349-362.

Grogan, R. M., and Bradbury, J. C., 1968, Fluorite-zinc-lead deposits of the Illinois-Kentucky mining district, *in* Ridge, J. D., ed., Ore deposits of the United States (Graton Sales Volume): New York, American Institute of Mining, Metallurgical and Petroleum Engineers, v. 1, p. 370-399.

Grogan, R. M., and Shrode, R. S., 1952, Formation temperatures of southern Illinois bedded fluorite as determined from fluid inclusions: Am. Mineralogist, v. 37, p. 555-566.

Hall, W. E., and Friedman, I., 1963, Composition of fluid inclusions, Cave-in-Rock fluorite district, Illinois, and upper Mississippi Valley zinc-lead district: ECON. GEOL., v. 58, p.886-911.

Hanor, J. S., 1979, The sedimentary genesis of hydrothermal fluids, *in* Barnes, H. L., ed., Geochemistry of hydrothermal ore deposits: New York, Wiley, p. 137-172.

Harder, V. M., 1986, Fluorite: A new fission track age dating material [abs]: Geological Society of America Abstracts with Programs, v. 18, p. 173-178.

Haynes F. E., and Kesler, S. E., 1987, Chemical evolution of brines during Mississippi Valley-type mineralization: Evidence from east Tennessee and Pine Point: ECON. GEOL., v. 82, p. 53-71.

Heinrich, C. A., Pettke, T., Halter, W. E., Aigner-Torres, M., Audetat, A., Gunther, D., Hanttendorf, B., Bleiner, D., Guillong, M., and Horn, I., 2003, Quantitative multi-element analysis of minerals, fluid, and melt inclusions by laser ablation-inductively coupled plasma-mass spectrometry: Geochimica et Cosmochimica Acta, v. 67, p. 3473-3496.

Heyl, A. V., 1983, Geologic characteristics of three major Mississippi Valley Districts: in Kisvarsanyi, G., Sheldon, S. K., Pratt, W. P., and Koeing, J. W., eds., International conference on Mississippi Valley Type lead-zinc deposits: Proceeding volume: Rolla, University of Missouri-Rolla Press, p. 27-60.

Heyl, A. V., Brock, M. R., Jolly, J. L., and Wells, C. E., 1965, Regional structure of the southeast Missouri and Illinois-Kentucky mineral districts: U. S. Geol. Survey Bull. 1202-B, B1-B20.

Horn, E. E., and Amstutz, G. C., 1978, Fluid inclusions in fluorites of the Crystal mine, Illinois, U.S.A.: Miner. Mh., v. 7, p. 289-287.

Kendrick, M. A., Burgess, R., Leach, D., and Pattrick, R. A. D., 2002, Hydrothermal fluid origins in Mississippi Valley-type ore deposits combined noble gas (He, Ar, Kr) and Halogen (Cl, Br, I) analysis of fluid inclusions from the Illinois-Kentucky fluorspar district, Viburnum Trend, and Tri-State districts, Midcontinent United States: ECON. GEOL., v. 97, p. 453-469.

Linn, F., Bodnar, R. J., Becker, S. P., 2007, Experimental determination of Raman CH_4 symmetric stretching (ν_1) band position from 1-650 bar and 0.3-22 °C: Application to fluid inclusion studies: Geochimica et Cosmochimica Act, v. 71, p. 3746-3756.

Nelson, W. J., and Lumm, D. K., 1987, Structural geology of southeastern Illinois and vicinity: Illinois State Geological Survey, Circular 528, 70 p.

Paroli, R. M., and Butler, I. S., 1990, A handy indicator of resolution in Raman spectroscopy. *Appl*. *Spectrosc*. v. 44, p. 216-219.

Pinckney, D. M., and Haffty, J., 1970, Content of zinc and copper in some fluid inclusions from the Cave-in-Rock district, southern Illinois: ECON. GEOL., v. 65, p. 451-458.

Plumlee, G. S., Goldhaber, M. B., and Rowan, E. L., 1995, The potential role of magmatic gases in the genesis of Illinois-Kentucky fluorspar deposits: Implication from chemical reaction path modeling: ECON. GEOL., v. 90, p. 999-1011.

Richardson, C. K., and Pinckney, D. M., 1984, The chemical and thermal evolution of the fluids in the Cave-in-Rock fluorspar district, Illinois: mineralogy, paragenesis, and fluid inclusions: ECON. GEOL., v. 79, p. 1833-1856.

Ruiz, J., Richardson, C. K., and Patchett, P. J., 1988, Strontium isotope geochemistry of fluorite, calcite, and barite of the Cave-in-Rock fluorite district, Illinois: ECON. GEOL, v. 83, p. 203-210.

Shelton, K. L., Gregg, J. M., and Johnson, A. W., 2009 in press, Replacement dolomites and ore sulfides as recorders of multiple fluids and fluid sources in the southeast Missouri Mississippi Valley-type district: Halogen $^{87}Sr/^{86}Sr$-$\delta^{18}O$-$\delta^{34}S$ systematic in the Bonneterre Dolomite: ECON. GEOL., v. 104, 16 p.

Snee, L. W., and Hayes, T. S., 1992, $^{40}Ar/^{39}Ar$ geochronology of intrusive rocks and Mississippi Valley-type mineralization and alteration from the Illinois/Kentucky fluorspar district: U. S. Geological Survey Open-File Report 92-1, p. 59-60.

Spry, P. G., and Fuhrmann, G. D., 1994, Additional fluid inclusion data for the Illinois-Kentucky fluorspar district: Evidence for the lack of a regional thermal gradient: ECON. GEOL., v. 89, p. 288-306.

Spry, P. G., Koellner, M. S., Richardson, C. K., Jones, H. D., 1990, Thermochemical changes in the ore fluid during deposition at the Denton mine, Cave-in-Rock fluorspar district, Illinois: ECON. GEOL., v. 85, p. 172-181.

Stoffell, B., Appold, M. S., Wilkinson, J. J., McClean, N. A., and Jefferies, T. E., 2008, Geochemistry and evolution of Mississippi Valley-type mineralizing brines from the Tri-State and northern Arkansas districts determined by LA-ICP-MS microanalysis of fluid inclusions: ECON. GEOL., v. 103, p. 1411-1435.

Sverjensky, D. A., 1986, Genesis of Mississippi Valley-type lead-zinc deposits: Annual Review in Earth and Planetary Sciences, v. 14, p. 177-199.

Symons, D. T. A., 1994, Paleomagnetism and the late Jurassic genesis of the Illinois-Kentucky fluorspar district: ECON. GEOL v. 89, p. 438-449.

Trace, R. D., 1974, Illinois-Kentucky fluorspar district: Kentucky Geological Survey Series 10, Special Publication 22, p. 58-76.

Viets, J. G., Hofstra, R. T., Emsbo, P., 1996, Solute compositions of fluid inclusions in sphalerite from North American and European Mississippi Valley-type ore deposits: Ore fluids derived from evaporated seawater: Society of Economic Geologists Special Publication 4, p. 465-482.

Viets, J. G., and Leach, D. L., 1990, Genetic implications of regional and temporal trends in ore fluid geochemistry of Mississippi Valley-type deposits in the Ozark region: ECON. GEOL. v. 85, p. 842-861.

Weller, J. M., Grogan, R. M., and Tippie, F. E., 1952, Geology of fluorspar deposits of Illinois: Illinois State Geological Survey Bulletin, v. 76, p. 147.

Wenz, Z. J., 2011, Geochemistry and origins of Mississippi Valley-type mineralizing fluids from the Ozark Plateau: Unpublished Ph. D. dissertation, University of Missouri-Columbia.

Winter, J. D., 2001, An Introduction to Igneous and Metamorphic Petrology: Prentice Hall Inc, 697 p.

Zacharias, J., and Wilkinson, J., 2007, ExLAM 2000: Excel VBA application for processing of transient signals from laser ablation (LA-ICP-MS) of fluid inclusions and solid phases [abs]: ECROFI-XIX Biennial Conference on European Current Research on Fluid Inclusions, Bern, Switzerland, Abstracts.

Zartman, R. E., Brock, M. R., Heyl, A. V., and Thomas, H. H., 1967, K-Ar and Rb-Sr ages of some alkalic igneous rocks from the central and eastern United States: American Journal of Science, v. 265, p. 848-870.